Surface engineering on silicon based anode material for Li ion batteries

Okji Park

Interdisciplinary School of Green Energy

Graduated School of UNIST

Surface engineering on silicon based anode material for Li ion batteries

A thesis
submitted to the Interdisciplinary School of Green Energy
and the Graduated School of UNIST
In partial fulfillment of the
Requirements for the degree of
Master of Science

Okji Park

02.14.2013

Approved by

_____

Major advisor

Soojin Park

Surface engineering on silicon based anode material for Li ion batteries

Okji Park

This certifies that the thesis of okji Park is approved.

02.14.2013

Signature

_____

Thesis supervisor: SoojinPark

Signature

_____

Kyu Tae lee

Signature

_____

Nam-Soon choi

Abstract

The exhaustion of traditional energy and the deterioration of environment have been seriously hindering social development and daily life, especially transportation. Exploring more efficient and environmentally-friendly power devices has attracted tremendous attention in the recent 50 years. Among various devices, lithium-ion batteries (LIBs) have been considered the most promising one, in terms of high voltage, large specific capacity, and environmental friendliness. Accordingly, the LIBs are being extensively applied in growing diversities from laptops to hybrid electric vehicles (HEVs) and electric vehicles (EVs). However, the current LIB technology cannot satisfy the evergrowing demand for high-performance power sources. That is why many researchers have been exploring advanced materials including cathodes, anodes, and electrolytes to pursue higher energy and power density, longer life, and lower cost. Si, Sn, alloys, and M_nX_m-type compounds (where M = Fe, Co, Ni, Cu, Sn, etc., while X = O, S, N, etc.) are investigated as anode materials. Though all these active materials show considerable capability and promising prospects, many obstacles restrict their commercialization, including poor electronic conductivity, low Li^+ transfer efficiency, volume expansion/contraction during repeated cycling processes, and loss of active materials due to the corrosion of electrolytes or/and collapse of the stable structure. To overcome these troublesome obstacles, researchers have proposed various feasible strategies, such as optimizing the crystalline lattice of active materials by doping cations or anions, reducing particles to a suitable scale to offer enhanced electron/ Li^+ conductivity and reactivity, combining active materials and other active/inactive materials together for complementary strengthening, especially surface coating and core–shell structures.

In this study, we researched carbon-silicon composites and Ti_xSi_y-coated Si for anode materials. These enhanced electrochemical performances were compared with bare carbon and bare silicon. These synthetic approaches open up a way to make other composites of anode materials for high performance LIBs.

Part 1: Introduction

1. Surface coating of anode material for Li ion batteries

1.1 Carbon anode materials

Solid-electrolyte-interface (SEI) film on a carbon surface prevents the direct contact of the compounds via lithium intercalation with the electrolytes so that it is maintaining stability of carbon and a smooth intercalation and de-intercalation of lithium.[1, 2] Moreover, it is porous so that lithium ions can move from the electrolyte solution into the carbon.

In contrast, solvated lithium ions should be inhibited from intercalation. Their intercalation will lead to exfoliation of graphite and a consequent destruction of the graphite structure because the size of solvent molecules is much greater than that of lithium ions.[2] So, surface structures of carbon materials are important to its formation and consequently the electrochemical performance. Recent research on the surface coating focus on deposition of metals and metal oxides, coating with polymers and coating with other kinds of carbons.

1.1.1 Polymer coating

Polymers can be divided into electro-active and electro-inactive polymers. Former electro-active polymers include polypyrrole, polythiophene, and polyaniline, and so on.[3-5] In the case of polypyrrole, it can be coated by an in-situ polymerization technique and its coating reduces the charge-transfer resistance and overall polarization resistance. Meanwhile, the thickness of SEI film is also decreased although the reason is still unknown, and the consumed amount of lithium to form SEI film during the first cycle is reduced. Consequently, polymer coating improves capacity, rate capability, coulombic efficiency and cycling life in compare with bare graphite.[3]

In the case of polythiophene, its coating steps are multiple. Firstly, its coating also diminishes the exposure of the active sites to the electrolytes and irreversible capacity. Secondly, it provides good conductivity and the formed composite posses a good electronic network. As a result, a pressing process can be skipped the assembly line and this process will save cost for the production of lithium ion battery. Thirdly, it acts as a binder due to good elasticity. Therefore, commercially available binder, insulating fluorine-containing polymers such as polyvinyldifluoride to achieve good and stable contact of particles of active materials during cycling, is not necessary. Finally, lithium can reversibly dope in polythiophene though the reversible doping amount of lithium is low, about 44 mAh/g, and the reversible lithium capacity of its composite increases only slightly.[4]

Different polyanilines, such as protonated polyaniline, emeraldine base and emeraldine salt, have been tried and enhances like to those observed with PPy and polythiophene have been achieved.[5]

To improve the cycling life and reduce the irreversible capacity, ionically conductive copolymers were coated.[6] For instance, it can be encapsulated on the surface of natural graphite particles via

radiation-initiated polymerization, and the composite enhances cycling life and initial coulombic efficiency in compare with bare natural graphite. The encapsulation suppresses structural changes due to co-intercalation of the solvated lithium ions and assures stable electrode impedance during the cycling.[6] The polyacrylonitrile coating can also enhance the electrochemical performance.[7]

Later, electro-inactive polymers such as polyelectrolytes like gelatin and cellulose can improve the electrochemical performance of carbon anode materials, and their good effects are the following: (i) These polymers act as binders so that it don't need to fluorine-containing binder to ensure the anode materials to be mechanically stable during cycling.[5, 8-10] And (ii) since SEI film is formed uniformly, the irreversible capacity is decreased in the first cycle. Growth of the film is governed by the presence of the polyelectrolyte molecules. [5, 8, 9]

However, the efficiency of pretreatment associate with the polyelectrolyte species, the gelling power, the concentration and the pH of its solution for the pre-treatment procedure.[5] The minimized exposure of the active sites to the electrolyte solution perhaps increases in the coulombic efficiency.

These composites can enhance electrochemical performance with regard to coulombic efficiency in the first cycle, the cycling behavior, the reversible capacity and the rate capability. The other polymers also can be used for coating materials if these provide the same or other good effects.

1.1.2 Metal and metal oxide deposition

In case of propylene carbonate (PC)-based electrolytes, a decomposition of PC result in electrolyte solution intercalate into graphite instead of lithium, so that graphene sheets can be exfoliated.[11, 12] Moreover, the carbon active sites at the edge planes are remained. Consequently, the performance of graphite in PC-based electrolytes is seriously decreased. Depositing metals and metal oxides is a good solution to enhance its electrochemical performance.

The nano-sized nickel (10 wt%) is deposited on a graphite surface, and sodium hypophosphite is used as reduction agents. This deposition covers graphite surfaces and prevents the exposure of the edge surfaces into the electrolyte solution. So, the exfoliation of the graphene layers and gas evolution are extremely minimized. Consequently, the charge–discharge performance is enhanced and the explosion by the large production of gases is escaped.[13] Moreover, metals such of Ni are good conductors. And it enhances diffusion coefficients of the lithium ions and exchange current densities. And, it minimizes the surface film resistance and charge-transfer resistance compared to bare graphite. The composite exhibits less capacity loss over a 10-day storage period and good electrochemical performance at large current or high-rate capability.[14]

Tin can also be deposited on the graphite surfaces so as to enhance the reversible capacity and to avoid the exposure of the active edge sites to the electrolyte solution.[15, 16] Its electrochemical performance is affected with the loading amount of tin and the heating temperature since the heating

can convert Sn in the composites from amorphous to crystalline. It offers higher capacity because tin can be an additional host for reversible lithium storage.[17] Moreover, it enhances rate capability, coulombic efficiency, and a longer cycle life compare with bare graphite.[16] In some cases, Sn leads to an irreversible capacity loss in the first cycle, because a mechanism similar to the formation of the SEI film on the carbon surfaces.[15]

Other metals such as Zn, Ag, and Al can also be deposited on the graphite surface.[18-22] Their effects are similar with the above-mentioned examples. For instance, Ag and graphite composite improves the rate capability, the reversible capacity and the cycling behavior because of the increase in conductivity and the incorporation of an additional lithium storage site.[19,20] Also, Al and graphite composite enhances the cycling performance and the rate capability because of a decrease in charge-transfer resistance, which is shown in Figure 1.1.[21]

These metals are usually deposited on the carbon surfaces without selectivity in surface active sites. By dipping graphite into aqueous solutions of metal salts and subsequent heating at 600 ◦C under an argon atmosphere, the metals ions such as copper and silver are selectively concentrated on the reactive sites at the graphite surface, and are turned into metallic and/or carbidic nanoparticles to cover and/or remove these active sites. The amount of water absorbed by the composites under high humidity condition (about 1000 ppm H_2O) is still little because the number of active sites on the surfaces of the composites is decreased by this selective deposition. The composites display still a good electrochemical performance including high specific capacity in the first cycle and excellent cycling, as shown in Figure 1.2.[23-25] Figure 1.3 shows how SEI film is formed on graphite surface.[26] The graphite absorbs much water under high humidity since the active sites exist on graphite surfaces. Because of the presence of water, the SEI film on graphite surface is much loosed and solvated lithium ion can intercalate into graphite leading to exfoliation of graphite sheets and consequent destruction. When the active sites on graphite surface are removed, the graphite absorbs little water under high humidity. Consequently, good SEI film is formed, and leads to good cycling behavior.

Oxides such as SnO, SnO2 and MxO (M = Cu, Ni, Fe and Pb) can also be deposited onto the surfaces of graphitic carbon, and it act effectively.[15, 27, 28] For instance, composite of SnO and graphite offer enhanced electrochemical performance, including higher reversible capacity, longer cycle life and better rate capability, compared to bulk SnO or their mechanical mixtures.[15] However, their irreversible capacity loss is high in the first cycles due to electro-reduction reaction of the oxide precursors converted into metals. When the surfaces of the well-used graphitic carbon, usually called MCMBs (mesocarbon microbeads) are deposited with tin oxide, improves the reversible capacity.

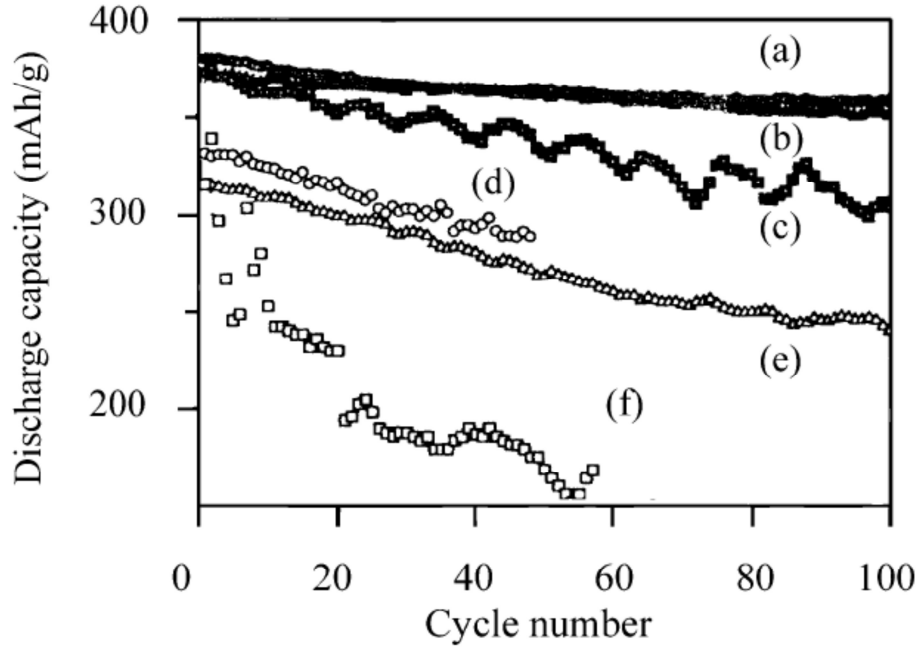

Figure1.1. Cycling performance of natural graphite (curves d, e and f) and of Al-treated sample (curves a, b and c): circles, triangles and rectangles represent 0.2 C, 0.5 C and 1 C rate, respectively.[21]

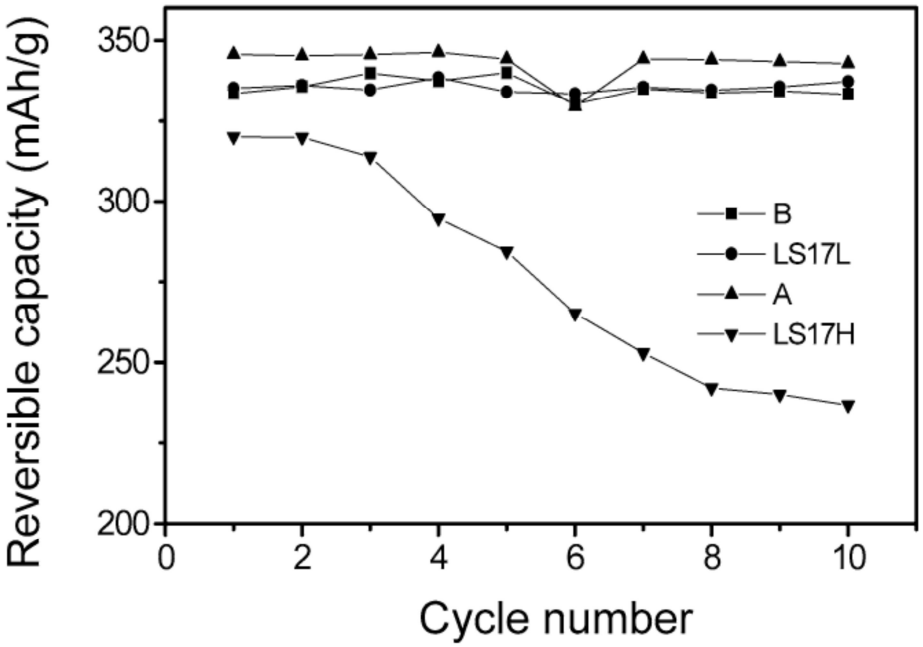

Figure1.2. Cycling behavior of natural graphite LS17 (curve LS17H) and of the prepared composites of LS17 deposited with 10.2 wt% Cu (curve A) and 8.6 wt% Ag (curve B), when the anode materials were assembled into cells under high humidity condition (about 1000 ppm H_2O). For comparison cycling behavior of LS17 under low humidity (below 100 ppm) is also shown as curve LS17L.[25]

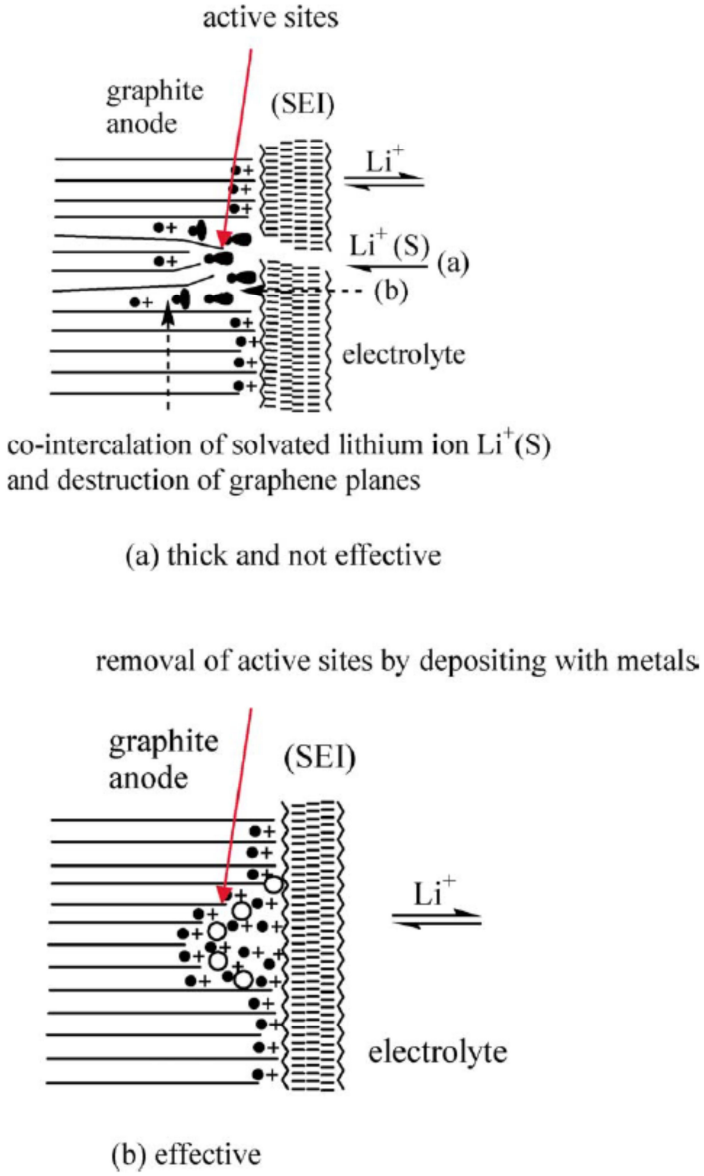

Figure1.3. Schematic diagrams of the solid-electrolyte-interface (SEI) film formed at the surface of bare graphite and the composites of graphite selectively deposited with metals: (a) Bare graphite processed under high humidity, and (b) Composite processed under high humidity: •+: intercalated lithium ion; :LiOH; :solvated Li+; ○: metal element. [26]

But, its capacity fades with cycling because of the serious volume change of tin oxide by lithium intercalation and deintercalation. This problem can be relieved by deposition of copper because copper acts as an inactive matrix and offers a buffer against the volume change.[27]

The metal deposition can provide towardly actions but, an excess of metals lead to adverse effects because of the aggregation of metals. Even though metaloxides provide improved capacity, the unfavorable irreversible reactions of metal oxides with Li producing Li_2O hinder its practical application.

1.1.3 Coating with other forms of carbon

In the case of graphitic carbon, we usually regard an ideal electrolyte solvent not PC but EC.[1, 11, 12] But, the melting point of EC(38 ◦C) is higher than that of PC(-49◦C).[1] To broaden the application fields of liquid electrolyte based lithium ion batteries, one should attempt to enhance their performance at low temperatures such as−30 ◦C. Coating with other forms of carbon maybe become one way. Coating with additional carbons can be processed by several methods: (i) Direct thermal vapor decomposition of organic molecules of organic molecule at 1000◦C can convert from carbon to graphite[28,29] ; (ii) In order to produce carbon, graphite was dispersed into a tetrahydrofuran/acetone solution containing coal tar pitch and then heat treatment at 1000 ◦C in an argon atmosphere[30]; and (iii) graphite and polymers such as poly(vinyl chloride) mixtures was heated at 800–1000 ◦C in an argon flow.

These coating prevent exposure of active site to the electrolytes so that the decomposition of PC is much decreased, and an effective SEI film is formed.[28, 29, 31] As a result, co-solvent of dimethyl carbonate and PC don't occur the decomposition of PC and the exfoliation of graphite layers.[28] These coating improves electrochemical performance including the reversible capacity, the cycling behavior and the coulombic efficiency in the first cycle in comparison with bare natural graphite.[28, 31]

From the cyclic voltammograms at different scan rates, the carbon "shell" as well as graphite "core" can be identified, indicating that shell also contributes to the reversible lithium capacity.[29] But, these coating should be avoided high pressure during the process of rolling and pressing because it will destructure carbon shell and expose graphite core to the PC-based electrolyte again.[31]

Regarding the change in the surface area after coating, it depends on the coating materials. In the case of poly(vinyl chloride) composite, its specific surface area is increased.[31] On the other hand, in the case of coal tar pitch composite, pores of <10 nm in the graphite are coated by the coke component leading to less surface area than that of the bare graphite. However, theses display similar enhancement in the electrochemical performance, which explain that the irreversible capacity increases with the specific surface area exclusively when the carbons have the same characteristics.

In the case of coke carbon anode, these are coated with pitch carbon by heat treatment. These composite offer a reversible lithium capacity of 400 mAh/g, but the pitch carbon and the coke carbon

offer only an first reversible capacity of about 310 and 295 mAh/g between 0 and 1.5 V vs. Li^+/Li, respectively.[32] When MCMBs, these are modified with carbons from polymers to get enhancements.[33] For instance, the carbon coating with epoxy resin enhances the electrochemical performance including the charge–discharge capacity and the cyclability.

Coating with additional carbons is effective, but further research is remained. Also, new and better carbon composite can show better electrochemical performances.

1.2 Other anode materials

There are many other anode materials such as novel alloys, nitrides, tinbased composite oxides, TiO_2, nano-oxides, fluorides and phosphides.[1, 34-38] Recently, it was reported that nano-tin alloy coating could improve its electrochemical behavior.[39] The alloy anodes have problem of drastic volume expansion during cycling so that pulverization is occurred. Consequently, the contact between the active material and current collector becomes loose, and it show lousy cyclic characteristics.

Even nanomaterials, this problem still remained, though it is relieved to some degree. Coating is one good solution to enhance their cycling life. For instance, polyaniline can alleviate volume changes during cycling. In addition, it has a high binding energy to protect anode cracking, and is electronically conductive that offers additive low interfacial lithium insertion/extraction impedance. As a result, its coating enhances the stability of nano-sized tin during cycling and leading to a good reversible intercalation and de-intercalation of lithium.[39] In case of silicon particles (about 1–2 μm), it was coated with carbon by thermal vapor deposition. This coating can decrease the damage caused by the large volume change of the formation of Li*x*–Si alloys, and the cycling is much enhanced.[40]

Whereas, other anode materials such as nano-oxides and fluorides exhibit high reversible capacity of >1000 mAh/g. However, there are disputes on the interpretation of the lithium storage. From these results, we may insist that changes of the surface structures were crucial to their stable cycling.[34, 35, 41]This presents that the surface modification is crucial for the lithium storage.

The nanomaterials can be enhanced in cycling by coating a thin layer of carbon.[42-44]This process is schematically shown in figure 1.4, which dissimilar to the above-mentioned ways to coat carbon. One detailed example is as follows: OP_9 (1.2 g, a neutral surfactant) was dispersed in deionized water (200 ml) to form micelles. Titanium oxide nanoparticles (2.5 g with hydrophobic surface) were added and ultra sonicated for 30 min to achieve uniform dispersion. A mixture of 2,2'-azobis(isobutyronitrile) (0.015 g, initiator) and distilled acrylonitrile (3.0 g, monomer) was added.

Degassing was carried out for 1 hr under gentle stirring, then the temperature was increased to 60 ◦C and the mixture was polymerized for 12 h under argon atmosphere to form a core-shell shaped TiO_2/polyacrylonitrile precursor. After precipitating and drying, the TiO_2/PAN precursor was heat treated at 800 ◦C to turn the PAN shell into the carbon shell, thus a TiO_2/C nanocomposite was

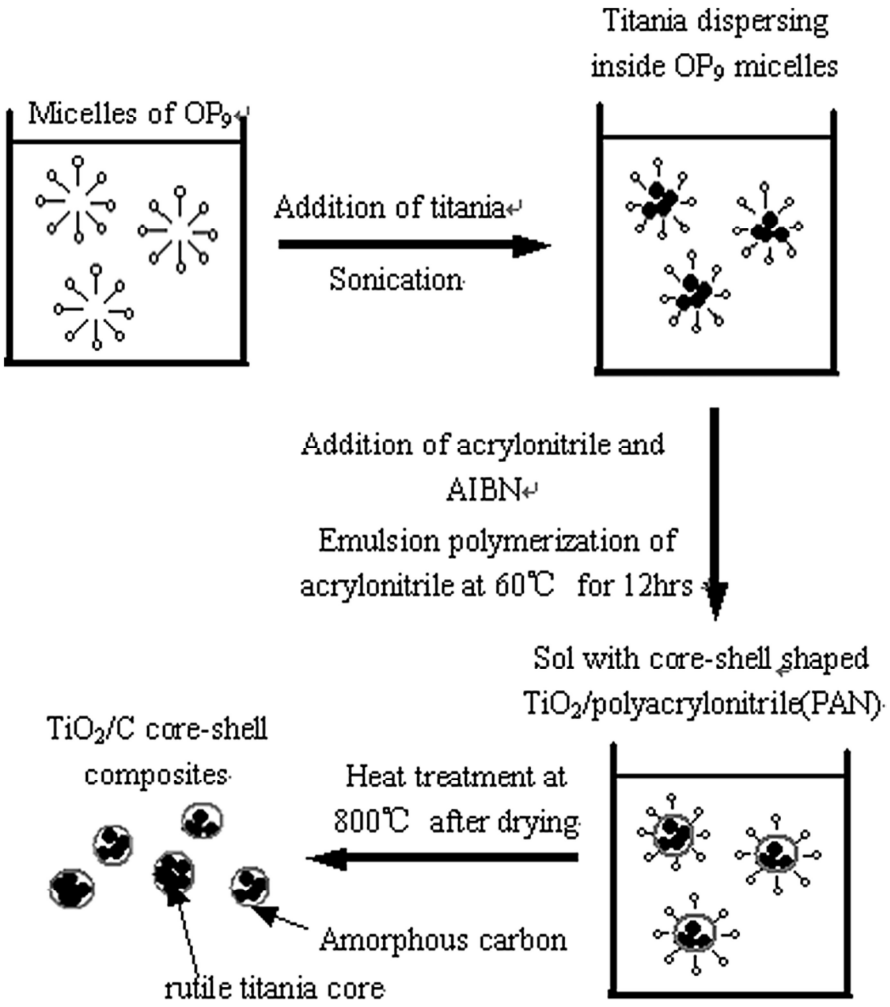

Figure1.4. Preparation process of TiO2/C core-shell nanocomposites.[42]

synthesized. The nanocomposite presents better cycling performance and higher diffusion coefficients of lithium ions compared with the virginal TiO_2 nanoparticles, which is due to the existence of conductive carbon\ shells and their close combination with the cores. This method shows great promise to improve the cycling behavior and kinetics of Si with high reversible capacity. [44, 45]But, it was known that the coating effects hang on the shape of nanoparticles. When they are spherical or nearly spherical, it will be much easier and good effect can be achieved.[45]

1.3 References

[1] E. Peled, D. Golodnitsky, J. Penciner, The anode/electrolyte interface, in: J.O. Besenhard (Ed.), Handbook of Battery Materials, Wiley–VCH, Weinheim, **1999**, pp. 419–456

[2] D. Aurbach, B. Markovsky, I. Weissman, E. Levi, Y. Ein-Eli, *Electrochim. Acta.* **1999**, *45,* 67-68

[3] S. Kuwabata, N. Tsumura, S. Goda, C.R. Martin, H. Yoneyama, *J. Electrochem. Soc.* **1998**, *145,* 1415-1420

[4] B. Veeraraghavan, J. Paul, B. Haran, B. Popov, *J. Power Source.,* **2002**, *109,* 377-387.

[5] M. Gaberscek, M. Bele, J. Drofenik, R. Dominko, S. Pejovnik, *J. Power Sources.* **2001** , *97/98* 67-69.

[6] Q. Pan, K.K. Guo, L.Z. Wang, S.B. Fang, *Solid State Ionics.* **2002,***149,*193-200.

[7] K.K. Guo, Q.M. Pan, S.B. Fang, *J. Power Sources.***2002**, *111,*350-356.

[8] J. Drofenik, M. Gaberscek, R. Dominko, M. Bele, S. Pejovnik, *J. Power Sources.***2001**, *94,* 97-101.

[9] M. Gaberscek, M. Bele, J. Drofenik, R. Dominko, S. Pejovnika, *Electrochem. Solid-State Lett.* **2000**, *3,* 171-173.

[10] M. Bele, M. Gaberscek, R. Dominko, J. Drofenik, K. Zupan, P. Komac, K. Kocevar, I. Musevic, S. Pejovnik, *Carbon.* **2002**, *40*, 1117-1222.

[11] E. Peled, D. Golodnitsky, J. Penciner, The anode/electrolyte interface, in: J.O. Besenhard (Ed.), Handbook of Battery Materials, Wiley–VCH, Weinheim, 1999, pp. 419–456,

[12] D. Aurbach, B. Markovsky, I. Weissman, E. Levi, Y. Ein-Eli, *Electrochim. Acta.* **1999***, 45,* 67-86

[13] P. Yu, J.A. Ritter, R.E. White, B.N. Popov, *J. Electrochem. Soc.* **2000***, 147,* 1280-1285.

[14] P. Yu, J.A. Ritter, R.E. White, B.N. Popov, *J. Electrochem. Soc.* **2000***,147*, 2081-2085.

[15] T. Takamura, K. Sumiya, J. Suzuki, C. Yamada, K. Sekine, *J. Power Sources.* **1999***, 81/82*, 368-372.

[16] B. Veeraraghavan, A. Durairajan, B. Haran, B. Popov, R. Guidotti, *J. Electrochem. Soc.* **2002***, 149*, A675-A681.

[17] Y.P. Wu, C. Wan, C. Jiang, J. Li, *Chin. J. Power Sources.* **1999**, *23,* 191.

[18] J. Lee, R. Zhang, Z. Liu, *J. Power Sources.* **2000***, 90*, 70-73.

[19] H. Momose, H. Honbo, S. Takeuchi, K. Nishimura, T. Horiba, Y. Muranaka, Y. Kozono, *J. Power Sources,* **1997** ,*68,* 208-211.

[20] K. Nishimura, H. Honbo, S. Takeuchi, T. Horiba, M. Oda, M. Koseki, Y. Muranaka, Y. Kozono, H. Miyadaera, *J. Power Sources.* **1997***, 68* , 436-439.

[21] S. Kim, Y. Kadoma, H. Ikuta, Y. Uchimoto, M. Wakihara, *Electrochem. Solid-State Lett.* **200** *,4* ,A109-A112.

[22] T. Takamura, Bull. *Chem. Soc. Jpn.* **2002**, 75, 21-44.

[23] Y.P. Wu, C. Wan, C. Jiang, E. Tsuchida, *Electrochem. Comm.* **2000***, 2*, 626-629.

[24] Y.P. Wu, C. Jiang, C. Wan, R. Holze, *J. Power Sources.* **2002***, 112*, 255-259.

[25] Y.P. Wu, C. Jiang, C. Wan, R. Holze, *Carbon* . **2003**, *41*, 437-443.

[26] L.J. Fu, Y.P. Wu, H.Q. Wu, R. Holze, *Electrochem. Solid-State Lett.* **2005***, 8*, A456-A458.

[27] J.K. Lee, D.H. Ryu, J.B. Ju, Y.G. Shul, B.W. Cho, D. Park, *J. Power Sources.* **2002***, 107,* 90-101.

[28] M. Yoshio, H. Wang, K. Fukuda, Y. Hara, Y. Adachi, *J. Electrochem. Soc.* **2000**, *147*, 1245-1250.

[29] H. Wang, M. Yoshio, *J. Power Sources.* **2001**, *93*, 123-129.

[30] S. Yoon, H. Kim, S.M. Oh, *J. Power Sources.* **2001***, 94,* 68-73.

[31] H. Lee, J. Baek, S. Jang, S. Lee, S. Hong, K. Lee, M. Kim, *J. Power Sources.* **2001**,*101,* 206-212.

[32] Y. Sato, Y. Kikuchi, T. Nakano, G. Okuno, K. Kobayakawa, T. Kawai, A. Yokoyama, *J. Power Sources.* **1999**, *81/82*, 182-186.

[33] J.S. Kim, W.Y. Yoon, K.S. Yoo, G. Park, C.W. Lee, Y. Murakami, D. Shindo, *J. Power Sources.* **2002***,104*, 175-180.

[34] P. Poizot, S. Laruelle, S. Grugeon, L. Dupont, J.M. Tarascon, *Nature.* **2003***, 407*, 496-499.

[35] H. Li, G. Richer, J. Maier, *Adv. Mater.* **2003***,15*,736-739.

[36] P. Balaya, H. Li, L. Kienle, J. Maier, *Adv. Func. Mater.* **2003***, 13,* 621-625.

[37] D.C.S. Souza, V. Pralong, A.J. Jacobson, L.F. Nazar, *Science.* **2003** *, 296*, 2012-2015.

[38] Y.P. Wu, X.B. Dai, J.Q. Ma, Y.J. Chen, Lithium Ion Batteries: Applications and Practice, Chemical Industry Press, Beijing, **2004**.

[39] X.W. Zhang, C.S. Wang, A.J. Appleby, F.E. Little, *J. Power Sources.* **2002***, 109*,136-137

[40] N. Dimov, S. Kugino, M. Yoshio, *Electrochim Acta.* **2003***, 48*, 1579-1587

[41] J. Jamnik, J. Maier, *Phys. Chem. Chem. Phys.* **2003***, 5,* 5215-5220.

[42] L. J. Fu, H. Liu, H. P. Zhang, C. Li, T. Zhang, Y. P. Wu, R. Holze, H. Q. Wu. *Electrochem. Commun.* **2006***, 8,* 1-12.

[43] L.J. Fu, H. Liu, H.P. Zhang, C. Li, T. Zhang, Y.P.Wu, H.Q.Wu,, *J. Power Sources.* **2006***, 159*, 219–222.

[44] T. Zhang, L.J. Fu, H.P. Zhang, Y.P. Wu, H.Q. Wu, *Pure and Applied Chemistry.* ***2008****, 78*, 1889–1896

[45] L. J. Fu, H. Liu, C. Li, Y. P. Wu, R. Holze, H. Q. Wu. *Solid State Sciences*. **2006**, *8,* 113–128.

2: Core-shell structures

2.1 Si with carbon shell

Anode materials have several problems including low electronic conductivity, Li^+ diffusion and large volume expansion/contraction. For instance, Si-based materials have high theoretical capacities of approximately 4200 mAh/g (corresponding to the formation of $Li_{4.4}Si$ alloy), which is 11 times that of the commercialized graphite (372 mAh /g for LiC_6). But, the drastic volume expansion (up to 400%) takes place during alloy/dealloy processes so that pulverization and destruction of the electrically conductive network are occurred. Consequently, the practical application is restricted .[1, 2]

2.1.1 Si nanoparticles with carbon shells

In order to cover the strain and the structural integrity, numerous researchers have been tried to make Si-based composites in which Si is homogenously dispersed in active/inactive matrix. Regarding to matrixes, carbon materials are greatly promising candidate concerning high electronic conductivity, abundance, good elasticity, easy preparation and low cost. For instance, carbon-coated Si composites have been synthesized in various methods, displaying capacities from 500 to 900 mAh /g.[3-6] The transformation from bulk to nanostructures leads to higher interfacial areas, better covering of the lithiation/delithiation strain, and shorter path lengths for Li^+ transport. Meanwhile, it has not only higher irreversible capacity, but also side reactions from the active surface of nano-Si powder. The carbon shell can complement these disadvantages by restricting side reactions and aggregation during alloying/dealloying processes. Therefore, carbon coated nano-Si is most promising method to enhance the electronic conductivity and simultaneously overcome disadvantages of nano-sized Si.

In addition, the ball-milling process can be used for Si@C composites. However, such mechanical mixing leads to loose and inhomogeneous electrical contact. Ng et al. successfully produced carbon-coated Si nanocomposites by a spray-pyrolysis technique, in which nanocrystalline Si powders were homogeneously dispersed into the citric acid/ethanol solution in the weight ratio of 1 : 10 (Si/citric acid), via ultrasonication for 90 min. Subsequently the obtained solution was pyrolyzed in a vertical-type spray pyrolysis reactor in air, with a flow rate of 4 mL/ min. [7, 8, 73] The as-synthesized Si@C have good electrochemical performances including a high capacity of 1489 mAh /g and a high coulombic efficiency of over 99.5% even after 20 cycles. The long-time ultra sonication and pyrolysis processes were good for the acid coating and in-situ carbonization. Similarly, GaO et al. chose poly(cyclotriphosphazene-4,4-sulfonyldiphenol) (PZS) as the encapsulating polymer in order to its easy synthesis way, good interface compatibility with the inorganic phase and intrinsic thermosetting property that is good to avoid conglutination and incorporation of nanoparticles during the pyrolysis process (Figure2.1a).[9] A long-time ultrasonication greatly prevented agglomeration of the high-surface-energy nanoparticles in solvents. The improved cyclability of over 1200 mAh/g should be

associated with homogeneously distributed nano-Si particles in the amorphous carbon matrix.

For Si@C nanocomosites, the binding of Si and C is very important for the performance improvement. As soon as heat treatment, carbon layer was grown up densely since SiO_2 layer or covalent linkage promote these growth. Hu et al. realized that only hydrothermal reaction can prepare Si@SiOx/C nanocomposite.[10] This nanocomposite anode showed a large reversible capacity (1100 mAh/g) up to 50 cycles with vinylene carbonate (VC)-containing electrolytes. Su et al. have suggested core double shell Si@SiO_2@C nanocomposites by modifying the nano-Si surface with a well-proportioned Li_4SiO_4 layer before the carbon coating during a hydrothermal reactions(Figure 2.1b). [11] When acetone acts as the lubricant, Li metal and pure nano-Si were homogeneously mixed by ball milling. After sintering at 400 ^oC for 2 h under Ar atmosphere, Li_4SiO_4 layer formed and then was decomposed into SiO_2. Meanwhile, glucose was carbonized during the hydrothermal reaction to form the carbon layer. Modified Si by SiO_2 films was good for following C-coating that is attributed to hydroxyl groups yielded from hydrolysis of Li_4SiO_4. The equations of these reactions are as following:

$$4Li + 2O_2 + Si \rightarrow Li_4SiO_4 \qquad (1)$$

$$Li_4SiO_4 + 2H_2O \rightarrow SiO_2 + 4LiOH \qquad (2)$$

Furthermore, more core–shell Si@C nanocomposites were successfully prepared by dispersing nanocrystalline Si in carbon aerogels and subsequent carbonization, and display good reversible capacities (over 1000 mAh /g).[12]

2.1.2 Si nanowires and nanotubes with carbon shells

Compared to Si@C nanoparticles, Si@C nanowires and nanotubes core-shell anode materials provide good electronic transport and great accommodation for volume expansion, particularly when nanowires/ nanotubes directly and regularly grow on the current collector in LIBs.

For example, Kim et al. presented mesoporous Si@C core–shell nanowires (D: 6.5 nm).[13] The as-synthesized core–shell Si@C nanowires demonstrated an excellent initial charge capacity of 3163 mAh /g with a coulombic efficiency of 86% at a rate of 0.2 C (600 mA/g) between 1.5 and 0 V. Moreover, the capacity retention after 80 cycles was 87%, while the rate capability at 2 C (6000 mA/ g) was 78% of that at 0.2 C.

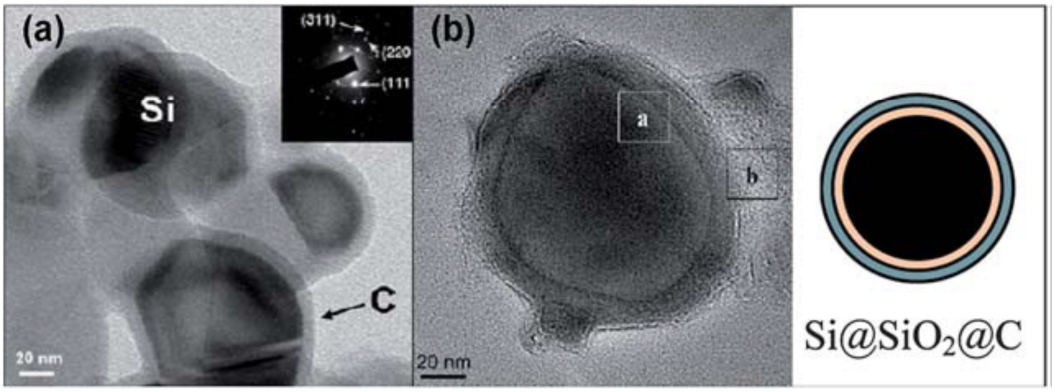

Figure 2.1 TEM images of Si@C (a) and Si@SiO_2@C (b). [9, 11]

Hertzberg et al. synthesized core–shell Si@C with an inner Si layer via SiH_4 decomposition at 500 ^oC.[14] The compressed Si tubes were attached to the CNT walls by electrical contact. After cycling, defects of CNT wall are very small and Si core shrinks, indicating reversible shape changes. This composite offers a capacity of 2100 mAh /g when Si content is 46 wt%.

In addition to carbon coating materials, core–shell 1D Si materials still displayed improved electrochemical behaviors. Cui et al. synthesized core (crystalline)–shell (amorphous) Si nanowires grown directly on stainless steel current collectors.[15] Since The lithiation potentials of crystalline Si different from amorphous Si, crystalline Si was chose as the core and amorphous Si as the shell. So, crystalline Si cores act as a mechanical support and an electrical conducting pathway while amorphous shells store Li^+ ions. Such core–shell nanowires showed a specific capacity of 1000 mAh/ g and cycle retention of 90% over 100 cycles.

Though core–shell Si@C composites displayed much improved specific capacities and high-rate stability, they have still obstacles for practical utilization because of their complicated preparation route, high cost, and low tap density.

2.2 Metal oxide with carbon shell

Poizot et al. have been exploring efficient metal oxide (MO) anode materials because metal oxides showed a high reversible capacity in LIBs.[16] Even though MO materials are diverse, most studies mainly focus on Fe_3O_4, SnO_2 and TiO_2 since these materials have low loss of electrochemical capability. The mechanism of Li storage in MO materials involves the formation and decomposition of Li_2O, accompanying the reduction and oxidation of metal nanoparticles. The conversion mechanism can be simply described as $MnOm + 2mLi^+ + 2me^-$ 4 $nM + mLi_2O$, in which MnOm except SnO_2 and TiO_2. However, the drastic volume expansion during these repeated processes, low coulombic efficiency and poor electronic conductivity (except Fe_3O_4) disturb their practical applications. The association of nanosization and core–shell structures offers enhanced performance because of a decreased Li+ ion transfer length, increased electronic conductivity and alleviated volume change.

2.2.1 Fe_3O_4 with carbon shells

Iron oxide (Fe_3O_4) anode has a high theoretical capacity (928 mAh/g), good stability, low cost, environmental friendliness, and especially high electronic conductivity which is very outstanding among MOs (see Table 1). The main problem of Fe_3O_4 is the large expansion during cycling and leads to pulverization as well as the low coulombic efficiency at first. Carbon coating is good strategy for alleviating the volume expansion and maintaining the structure integrity.

Table 1. Electrochemical properties of main active and coating materials [43]

	Crystal Structure	Limiting Composition	Theoretical Capacity (mAh/g)	Volume Strain Δv/v	s (S/cm)	D_{Li^+} (cm^2/s)	Refs
Si	diamond cubic	$Li_{4.4}Si$	4200 >	300%	$1.56x10^{-5d}$	10^{-13}	46–48
Sn	tetragonal	$Li_{4.4}Sn$	994	260%	$9.17x10^{4}$	10^{-8}–10^{-7}	44,49
Fe_3O_4	spinel	Fe^0 + Li2O	928	80.30%	10^{2}	—	47,50,51
SnO_2	rutile	$Li_{4.4}Sn$	783	—	10^{-3}	—	
TiO_2	anatase	$Li_{0.5}TiO_2$	168 <	4%	10^{-10}	10^{-6e}	41,45,52-54
	rutile					10^{-17e}-10^{-10e}	
graphite	layered	LiC_6	372	13.10%	10^{3}	10^{-11}-10^{-10}	44,47,55-57
amorphous C		—	—	—	10^{-2}-10	—	58
RuO_2	rutile	Ru^0 + Li_2O	806	—	10^{4}	—	59-62
Cu	—	—	—	—	$5.96x10^{5}$	—	57
graphene	layered	LiC_3	744	—	10^{6}	10^{-6}	56,63

[a] All the values were obtained at room temperature. [b] The theoretical capacities of LiMO2 (M ¼ Co, Ni, Mn) are based on the complete extraction of Liion, while the values of other materials correspond to the conversion from the original phase to the counterpart limiting composition. [c] ''–'' means that this value is not reported or not significant. d the resistivity of semiconductors depends strongly on the presence of impurities in the material. e The values were teste in c- and a-direction of crystalline TiO2, respectively.

Sun and coworkers introduced a one-pot hydrothermal reaction to synthesize metal oxide@C core–shell nanostructures. Water soluble metal salts are introduced into a clear solution of glucose or other soluble saccharides, and hydrolyze/dehydrate under ambient or hydrothermal conditions to form oxide (or hydroxide, complex oxide) nano- or microparticles (Step I). As-formed carbonaceous materials encapsulate former oxide particles to form a thin sheath (Step II), which is penetrable for small molecules such as amine or hydrazine. The oxide cores could react with the carbonaceous shell or other introduced chemical reagents to convert into core–shell nanostructures (Step III). Besides hydrolyzation, various chemical reactions can be introduced under the aforementioned hydrothermal conditions before the carbonization of saccharides. This significantly enriches the accessible core–shell structured nanoparticles .[17, 43]

Meanwhile, Wan's group implements partial reduction of monodispersed hematite nanospindles with carbon coatings under hydrothermal conditions for synthesis of carbon-coated Fe_3O_4 nanospindles.[18] Carbon layer of carbon-coated Fe_3O_4 nanospindles decrease side reactions, alleviates volume changes, and prevents the pulverization of the electrode. Moreover, the carbon layer can acts as electrically conductive networks because of high electronic conductivity. Consequently, Fe_3O_4@C nanocomposites offer high reversible capacities (745 mAh /g at 0.2 C and 600 mAh /g at 0.5 C), high coulombic efficiencies at first and substantially improved cycling behaviors and high rate capabilities in comparison with bare hematite spindles. Similarly, core–shell Fe_3O_4@C nanowires (Figure 2.2b) were synthesized by a microwave-hydrothermal reaction with polyethylene glycol (PEG-400) as a soft template and showed great electrochemical behavior.[19] In order to accommodate the volume expansion, Fe_3O_4@C is combined with the mesoporous structurefor large surface area and voids. Yuan et al. successfully produce mesoporous Fe_3O_4@C nanocapsules (Figure 2.2c) by using the FeOOH nanorods not hematite nanospindles.[20] Interestingly, sintering at 500 ^oC offers mesoporous structure and transformation from carbonaceous sheath to carbon shells. The mesopores in Fe_3O_4 nanorods relieve volume change of active materials, because it has more space for volume change, and release the stress on the carbon shells. The results showed necessity of carbon coatings to improve the electrochemical performance of nanostructured MOs as anode materials for LIBs.

2.2.2 SnO_2 with carbon shells

SnO_2 is also promising MO anode materials due to its high theoretical specific capacity (780 mAh /g). The mechanism of Li storage in SnO_2 can be described in equation (3) and (4). The irreversible reaction in equation (3) and the formation of SEI films cause a large irreversible capacity at first. Another serious problem is the capacity fading because of the drastic volumetric change during cycles that disturbs its practical application. Core–shell structures are good solution for these problems.

$$SnO_2 + 4Li^+ + 4e^- \rightarrow Sn + 2Li_2O \qquad (3)$$

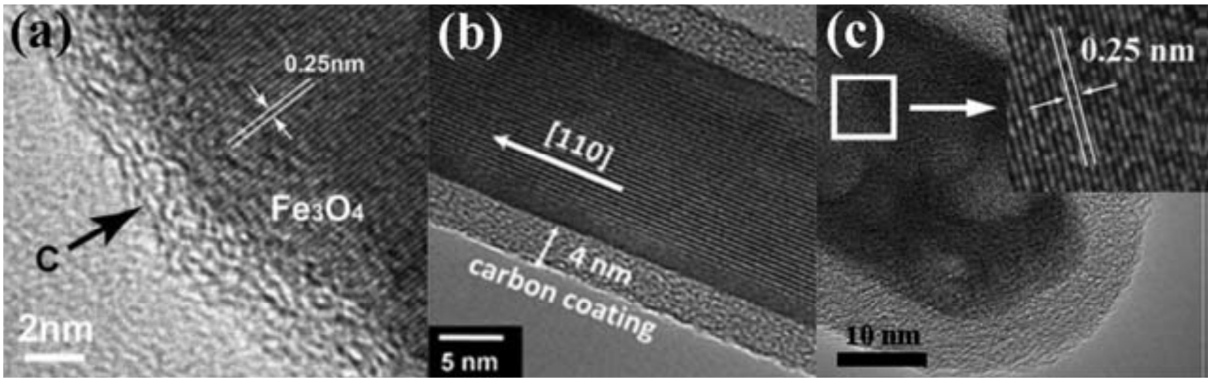

Fig.2.2. TEM images of Fe_3O_4@C nanospindles (a) [18] nanowires (b) [19], and mesoporous nanorods (c) [20]

$$Sn + xLi^+ + xe^- \rightarrow 4Li_xSn\ (0 \leq x \leq 4.4) \quad (4)$$

Recently, several core–shell SnO_2@C nanoparticles have been synthesized with various methods and offered better electrochemical performances.[40, 21-23] For instance, Zhang et al. introduced hydrothermal procedure for SnO_2@C core–shell nanochains with 3D superstructures.[40] The nanochain is composed of core–shell nanostructures with a homogenous carbon thickness of 10 nm (Figure 2.3) that the SnO_2 nanocores were fully coated and linearly joined one by one. The 3D network based on core–shell nanochains having a considerable capacity (over 600 mAh/g) at a high current density of 1104 mA/ g. Core–shell SnO_2@C hollow spheres were also studied by many researchers, since it alleviates the volume change, generates a rapid lithium transportation path and facilitate the high-rate capability, while the carbon shell offers better electronic conductivity.[24-26] Lou et al. synthesized coaxial SnO_2@C nanospheres with a SiO_2 template under hydrothermal conditions, and the template was removed by an alkaline solution.[25] Moreover, they prepared hollow SnO_2@C nanospheres by two steps of hydrothermal treatments.[26] Its ultrathin SnO_2 inner shell provides excellent cycling performance at high rates. Furthermore, the core–shell structure can combine with 1D nanomaterials to make SnO_2@Cnanofibers, CNT@SnO_2@C nanocables and SnO_2@V_2O_5 nanowires with high-rate capabilities.[27-29] Every result presents that the carbon shell enhances electrochemical performance of SnO_2 particularly when combining with hollow, 1D, or mesoporous structures.

2.2.3 TiO_2 with carbon shells

TiO_2 is a typical Li^+ intercalation compound instead of conversion reaction. The reaction can be ascribed as: $TiO_2 + xLi^+ + xe^- \leftrightarrow Li_xTiO_2$ ($0 \leq x \leq 1$) that occur a small volume change (<4%), and this is critical for the high-rate capability and long-life cycling. Moreover, TiO_2 can provide a low voltage (1.5 V vs. Li^+/Li) compared with that of $Li_4Ti_5O_{12}$ (1.9 V vs. Li^+/Li). But, the electronic conductivity of TiO_2 as an n-type semiconductor is low so that applications are limited. Composites of as-prepared TiO_2 and highly conductive materials such as C, Sn and PANI are good solution for this problem, particularly when combining with core– shell structures.[30, 31, 41] For example, Kim et al synthesized TiO_2@Sn core–shell nanotubes by thermal decomposition of $SnCl_4$ on TiO_2 nanotubes at 300 ^oC.[41] It displayed an excellent Li storage capability of 176 mAh /g even at high current rate of 4000 mA /g.

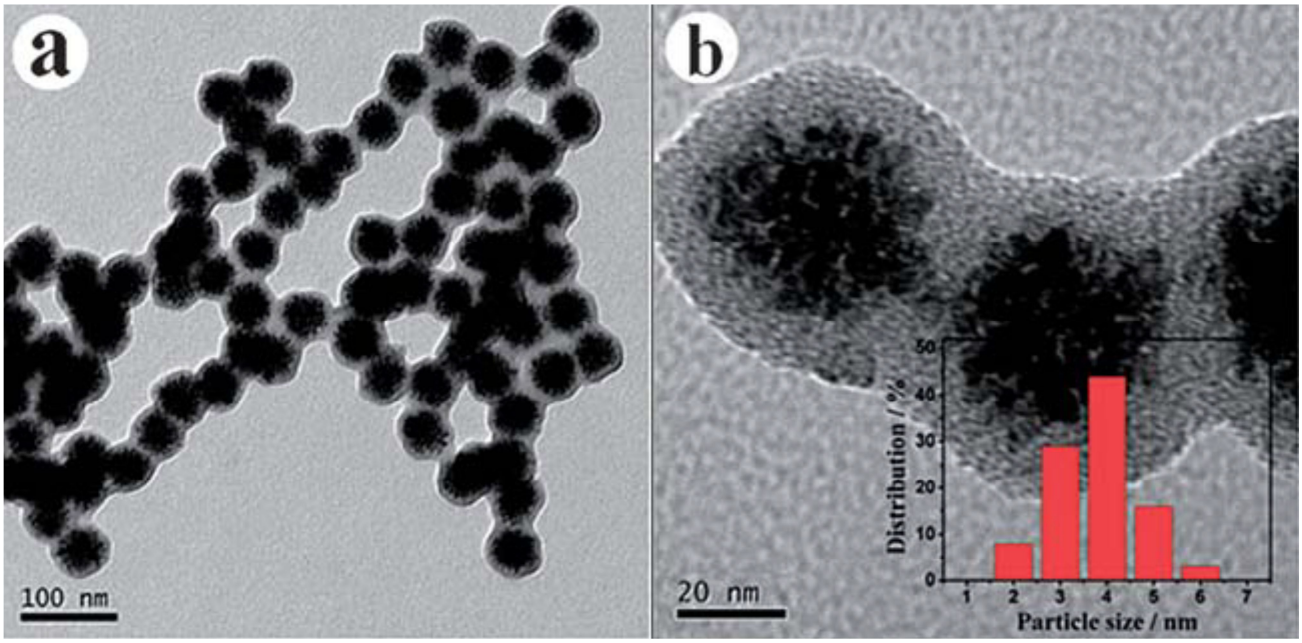

Figure2. 3. Typical TEM images of SnO_2@C nanochain-built superstructures. [40]

2.2.4 Other oxides with carbon shells

Numerous metal oxide materials have been thoroughly investigated as anode materials in LIBs.[32-38] However, only a few can be combined with carbon materials, because the high-valence metal can be reduced under the H_2 or CO atmosphere released during the traditional carbonization of polysaccharides at high temperatures (generally >40 ^{o}C).[42, 43] For instance, Fe_2O_3, Co_3O_4, MnO_2, MoO_3, CuO, and NiO can be gradually reduced into Fe_3O_4, CoO, MnO, MoO_2, Cu_2O and Ni metal, respectively. Higher temperatures can make counterpart metals as well. Following this line, some MO@C composites such as Fe_3O_4@C, and MnO@C, can be obtained from high-valence transition metal oxides coated with carbon precursors.[36,38,43] To decrease annealing temperatures can make the MO core with high valence and carbon shell simultaneously. For instance, MoO3@C nanobelts were synthesized by hydrothermal reaction following a heat treatment at 265℃ for 3 h in air.[42] The final product displays an outstanding cyclic stability and specific capacity of 1064 mAh/g at the 50th cycle due to the carbon coating on the nanobelts. SnO_2@C nanochains have been realized at a relatively high temperature (700 ^{o}C) through a low argon flow rate, during which trace oxygen was controllably released to maintain a chemical equilibrium for the following possible reaction process: $SnO_2 \leftrightarrow SnO \leftrightarrow Sn$.[39, 43] This low-flow-rate protecting concept opens up a way on synthesis of high-valance MOs@C composites.

2.3 References

[1] R. Teki, M. K. Datta, R. Krishnan, T. C. Parker, T.-M. Lu, P. N. Kumta and N. Koratkar, *Small*. **2009**, *5*, 2236–2242.

[2] J. R. Szczech, S. Jin, *Energy Environ. Sci.* **2011**, *4*, 56–72.

[3] K. Wang, X. He, L. Wang, J. Ren, C. Jiang and C. Wan, *Solid State Ionics*, **2007**, *178*, 115–118.

[4] P. Zuo, G. Yin and Y. Ma, *Electrochim. Acta*, **2007**, *52*, 4878–4883.

[5] U. Kasavajjula, C. Wang and A. Appleby, *J. Power Sources,* **2007**,*163*, 1003–1039.

[6] Y. Kang, M. Park, J. Lee and H. Liu, *Carbon*, **2007**, *45*, 1928–1933.

[7] S.-H. Ng, J. Wang, D. Wexler, K. Konstantinov, Z.-P. Guo and H.-K. Liu, *Angew. Chem., Int. Ed*., **2006**, *45*, 6896–6899.

[8] S. H. Ng, J. Wang, D. Wexler, S. Y. Chew and H. K. Liu, *J. Phys. Chem. C*, **2007**, *111*, 11131–11138.

[9] P. F. Gao, J. W. Fu, J. Yang, R. G. Lv, J. L. Wang, Y. N. Nuli and X. Z. Tang, *Phys. Chem. Chem. Phys*., **2009***, 11*, 11101–11105.

[10] Y.-S. Hu, R. Demir-Cakan, M.-M. Titirici, J.-O.M€uller, R. Schl€ogl, M. Antonietti and J. Maier, *Angew. Chem., Int. Ed*., **2008**, *47*, 1645–1649.

[11] L. W. Su, Z. Zhou and M. M. Ren, *Chem. Commun*., **2010**, *46*, 2590– 2592.

[12] Y. Xu, G. Yin, Y. Ma, P. Zuo and X. Cheng, *J. Mater. Chem*., **2010**, *20*, 3216–3220.

[13] H. Kim and J. Cho, *Nano Lett*., 2**008**, *8*, 3688–3691.

[14]B. Hertzberg, A. Alexeev and G. Yushin*, J. Am. Chem. Soc*., **2010**, *132,* 8548–8549.

[15] L.-F. Cui, R. Ruffo, C. K. Chan, H. Peng and Y. Cui, *Nano Lett*., **2009**, *9*, 491–495.

[16] P. Poizot, S. Laruelle, S. Grugeon, L. Dupont and J. M. Tarascon, *Nature*, **2000**, *407*, 496–499.

[17] X. Sun, J. Liu and Y. Li, *Chem. Mater*., **2006**, *16*, 3486–3494.

[18] W.-M. Zhang, X.-L. Wu, J.-S. Hu, Y.-G. Guo and L.-J. Wan*, Adv. Funct. Mater*., **2008**, *18*, 3941–3946.

[19]T. Muraliganth, A. V. Murugan and A. Manthiram, *Chem. Commun*., **2009**, *47*, 7360.

[20](a) S. M. Yuan, J. X. Li, L. T. Yang, L. W. Su, L. Liu and Z. Zhou, *ACS Appl. Mater. Interfaces*, **2011**, *3*, 705–709; (b) S. M. Yuan, Z. Zhou and G. Li, *CrystEngComm*, **2011**, *13*, 4709–4713.

[21]H. Qiao, Z. Zheng, L. Z. Zhang and L. F. Xiao, *J. Mater. Sci*., **2008**, *43*, 2778–2784.

[22]J. S. Chen, Y. L. Cheah, Y. T. Chen, N. Jayaprakash, S. Madhavi, Y. H. Yang and X. W. Lou*, J. Phys. Chem. C*, **2009***, 113*, 20504– 20508.

[23]R. Yang, W. Zhao, J. Zheng, X. Zhang and X. Li, *J. Phys. Chem. C*, **2010**, *114*, 20272–20276.

[24]X. W. Lou, D. Deng, J. Y. Lee and L. A. Archer, *Chem. Mater***., 2008**, *20*, 6562–6566.

[25]X. W. Lou, C. M. Li and L. A. Archer, *Adv. Mater.,* **2009,** *21*, 2536– 2539.

[26]Y.-S. Lin, J.-G. Duh and M.-H. Hung, *J. Phys. Chem. C*, **2010**, *114*, 13136–13141.

[27] L. Ji, Z. Lin, B. Guo, A. J. Medford and X. Zhang, *Chem.–Eur. J*., **2010**, *16*, 11543–11548.
[28]P. Wu, N. Du, H. Zhang, J. X. Yu and D. R. Yang, *J. Phys. Chem. C*, **2010**, *114*, 22535–22538.
[29]J. Yan, A. Sumboja, E. Khoo and P. S. Lee, *Adv. Mater.,* **2011**, *23*, 746–750.
[30]S. Shanmugam, A. Gabashvili, D. S. Jacob, J. C. Yu and A. Gedanken, *Chem. Mater.,* **2006**, *18*, 2275–2282.
[31]C. Lai, H. Z. Zhang, G. R. Li and X. P. Gao, *J. Power Sources*, **2011**, *196*, 4735–4740.
[32]L. Liu, Y. Li, S. M. Yuan, M. Ge, M. M. Ren, C. S. Sun and Z. Zhou*, J. Phys. Chem. C*, **2010**, *114*, 251–255.
[33]S.-L. Chou, J.-Z. Wang, D. Wexler, K. Konstantinov, C. Zhong, H.-K. Liu and S.-X. Dou, *J. Mater. Chem*., **2010***, 20*, 2092–2098.
[34]M. Y. Cheng and B. J. Hwang, *J. Power Sources*, **2010**, *195*, 4977– 4983.
[35]S. Shanmugam and A. Gedanken*, J. Phys. Chem. B*, **2006***, 110*, 24486–24491.
[36]B. Sun, Z. Chen, H.-S. Kim, H. Ahn and G. Wang, *J. Power Sources*, **2011**, *196*, 3346–3349.
[37]L.-Y. Jiang, S. Xin, X.-L. Wu, H. Li, Y.-G. Guo and L.-J. Wan, *J. Mater. Chem*., **2010***, 20*, 7565–7569.
[38] Z. Wang, J. S. Chen, T. Zhu, S. Madhavi and X. W. Lou, *Chem. Commun*., **2010**, *46*, 6906–6908.
[39] X. Yu, S. Yang, B. Zhang, D. Shao, X. Dong, Y. Fang Z. Li and H. Wang, *J. Mater. Ch*em., **2011**, *21*, 12295–12302.
[40] B. Zhang, X. Yu, C. Ge, X. Dong, Y. Fang, Z. Li and H. Wang, *Chem. Commun*., **2010**, *46*, 9188–9190.
[41] H. Kim, M. Kim, T. Shin, H. Shin and J. Cho, *Electrochem. Commun.,* **2008**, *10*, 1669–1672.
[42] Z. Chen, Y. Qin, K. Amine and Y. K. Sun, *J. Mater. Chem*., **2010**, *20*, 7606–7612.
[43] Liwei Su, Yu Jing and Zhen Zhou *Nanoscale*, **2011**, *3*, 3967–3983

Part 2: Carbon-silicon composites of anode material for Li ion batteries

1. Introduction

Lithium ion (Li-ion) batteries have long been considered as the most promising back-up power source for a wide variety of modern portable information technology equipment, following their commercial introduction in the early 1990s. So far, many kinds of anode materials have been investigated, such as graphitic carbons, disordered carbons, tin-based materials, nitrides, phosphides, and oxides.[1-18] However, only graphitic carbons are commercially available since the other materials have some disadvantages. For example, in the case of disordered carbons, though their preparation temperature is much lower than that of graphitic carbons and reversible capacity is much larger, there is a serious voltage hysteresis and capacity fading. Nowadays, owing to rapid advancement of electronic technologies, batteries are required to improve their capacity and cyclability. The latest research is focused on improving and searching for novel synthetic methods of the electrode materials [19-25] Recently, nanomaterials have attracted much interest as anodes for Li-ion batteries because of their larger reversible capacity, higher Li^+ diffusion coefficients, and better rate capability than conventional micrometer materials.[26-31]

In particular, silicon is regarded as one of the most promising candidates as anode material for Li-ion batteries. Its theoretical capacity (3750 mAh/g at room temperature) is much higher than that of the commercialized graphite (372 mAh/g).[19] However, the cycle performance of silicon is poor due to huge volume change during Li alloying/dealloying process, which results in pulverization of Si particles and eventual loss of Li storage ability.[35] To solve this problem, nanosized Si particles have been utilized and have achieved partial improvement by reducing the absolute volume change. Nevertheless, a new problem was encountered in nanomaterial, since nano-sized Si particles aggregate to larger ones during Li insertion/extraction, resulting in capacity loss.[36] Recently, soft matrixes for Si such as carbon, TiN and TiB_2, and silver were introduced to form composite with Si.[37-40] However, Si is still not stable and will separate with the soft matrixes, leading to poor cycling.

In this work, we report an effective method for synthesizing micro-/nanoscale hybrid CNT/Si core-shell (CNT@Si) composite via a facile magnesiothermic reduction process for high-performance Li-ion battery anode. When silica sol precursor was attached to acid-activated CNTs, microassembly of CNT/SiO_2 was formed. Subsequent magnesiothermic reaction of SiO_2 and Mg vapor led to the formation of micro-/nanoscale hybrid CNT/SiC/Si composite anode materials. Moreover, introduction of TiO_2 layer between CNT and SiO_2 and subsequent magnesiothermic reaction led to the preparation of CNT/TiC/Si composite materials. These anode materials showed a highly stable cycling performance and a high reversible capacity in LIBs.

2. Experimental

2.1 Materials

Chemical reagents ued for the synthesis of CNT/Si composites include tetraethyl orthosilicate (TEOS, Sigma-Aldrich), tetrabuthoxy titanium (Sigma-Aldrich), ammonium hyroxide (NH_4OH, Sigma-Aldrich), sulfuric acid (Samchun), nitric acid (Sigma-Aldrich), hyrochloric acid (Sigma-Aldrich), and Ethanol (J.T. Baker).

2.2 Functionalization of CNT

Pristine multi-walled carbon nanotubes (MWCNTs, with an average outer diameter of 15 nm) were activated by a reflux in strong acids as described previously,[15] producing oxygenated functional groups (–COOH, –OH, and C=O) on the CNTs surface.

2.3 Preperation of CNT/Si composites

The methodology employed in this study is outlined in Fig. 1. The resulting acid-oxidized MWCNTs (denoted as o-MWCNTs) become hydrophilic, which makes them well-dispersed in the reaction mixture. Typically, o-MWCNTs (0.2g) are ultrasonically dispersed into a fixed-volume mixture of ethanol (200 mL) and NH_4OH (12 mL, 25.0-28.0 wt%) for 30 min, followed by vigorous mechanical agitation for another 15 min to obtain a stable and homogeneous suspension. Subsequently, appropriate amount of TEOS is quickly added to achieve the desired volume ratio (vol.%) of TEOS with respect to ethanol, and kept stirring for 6 h. The whole reaction is carried out at room temperature. After the reaction, the mixture is centrifuged at a moderate speed (3500 rpm). In order to fully remove free silica sol precursors, the resultant sediment is filtered. The same procedure is repeated at least three cycles. The darkish product is obtained by filtration through a 0.45 μm cellulose membrane and dried in vacuum, yielding silica-coated MWCNTs (CNT-SiO_2). The CNT-SiO_2 is then heated in the furnace at 450 ^oC for 1 h under argon atmosphere to remove water and enhance structure stability of silica shell. Finally, silica (SiO_2) shell can be reduced by magnesium vapor at 700 ^oC for 1h to produce CNT/Si composite. Then, the formed magnesium oxide (MgO) was removed by hydrochloric acid (HCl).

2.4 Preperation of CNT/TiC/Si composites

In a typical synthesis, a 1mL of titanium tetrabutoxide and 1 mL of H_2O were refluxed in ethylene glycol/ethanol (120 mL/80 mL) at 100 ^oC for 6 h in the presence of 0.5g o-MWCNTs particles. After the reaction, the mixture is centrifuged at a moderate speed (3500 rpm). In order to fully remove free titania sol precursors, the resultant sediment is filtered. The same procedure is repeated at least three cycles. The darkish product is obtained by filtration through a 0.45 μm cellulose membrane and dried

in vacuum, yielding silica-coated MWCNTs (CNT-TiO_2). The CNT-TiO_2 is then heated in the furnace at 200 ^oC 1h and 400 ^oC for 1 h under argon atmosphere to remove water and enhance structure stability of silica shell. And then, above process of Si coating is operated.

2.5 Characterization and electrochemical test

The as-prepared CNT/Si composites were characterized by Transmission Electron Microscope (TEM, JEM-2100) and Scanning Electron Microscope (SEM, FEI) to investigate the morphology and thickness of the SiO_2 shell. For measuring the degree of reduction of silica shell, we used X-ray Diffractometer (XRD, Bruker)

Electrochemical cell test was performed using coin-type half cells (2016R type) by assembling in an argon-filled glove box. CNT/Si electrodes for the cell test were composed of Si active material (60 wt%), super P carbon black (20 wt%), and poly(acrylic acid)/sodium carboxymethyl cellulose (wt/wt, 50/50) binder (20 wt%). The electrolyte was composed of 1.3 M $LiPF_6$ in a mixture of ethylene carbonate/diethylene carbonate (ED/DEC, 30/70 vol. %) with 10 wt% fluoroethylene carbonate (FEC) additive. The cells were cycled at a rate of 0.1C in the range of 0.01 and 1.2 V. The cell test of CNT/Si-C and CNT/Ti/Si/C are processed same condition.

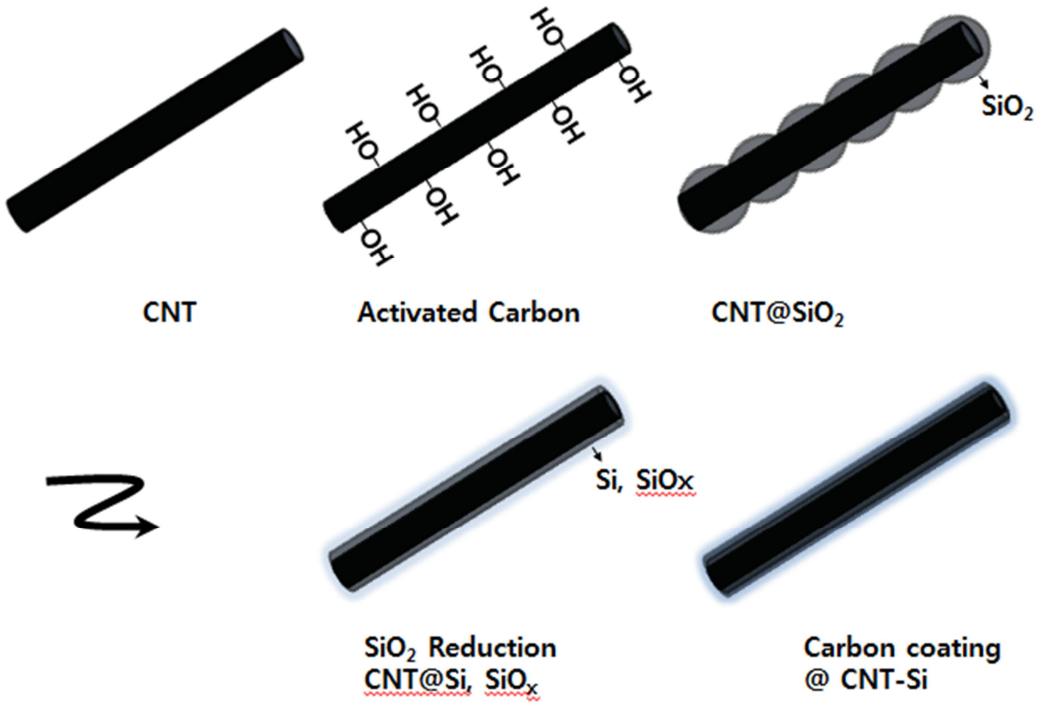

Figure3.1. Preparation process of CNT-Si core-shell nanocomposites

3. Result and discussion

TEM images of CNT and oxidized CNTs showed similar dimensions ranging from 10 to 20 nm in diameter (Figure 3.2a & 3.2b). When 9 mL of TEOS was added into ethanol solution containing 0.2 g oxidized CNTs, the amorphous SiO_2 layer having 15~20 nm thickness was conformally coated on the CNT surface (Figure 3.2c&3.2d). By controlling the amounts of NH4OH catalyst and TEOS, the thickness of SiO_2 layer was tuned. TEM images of CNT/SiO_2 core/shell structures (Figure 3.3(a-g)) showed that the thickness of silica shell when amounts of NH_4OH and silica precursor are controlled. The amounts of NH_4OH were controlled from 9 mL to 48 mL to obtain thickness of 15~20 nm without aggregation of SiO_2 sol. NH_4OH acts as catalyst so that it is crucial to tune thickness of SiO_2 shell. The amounts of NH_4OH and silica precursor were decreased to get desired thickness. However, when these were decreased to NH_4OH of 9 mL and TEOS of 8 mL, CNT were not entirely coated. Therefore, we took minimal condition of NH_4OH/ TEOS (12 mL/9 mL) for SiO_2 coating (Figure 3.3g).

Interestingly, the CNT/SiO_2 core/shell structure was self-assembled in microscale during the SiO_2 coating process due to the aggregation of SiO_2 sol in the presence of NH_4OH catalyst, as shown in SEM image of Figure 3.4a. From the energy dispersive X-ray spectroscopy (EDAX) analysis, 42 wt% silica contents was detected (Figure 3.4b).

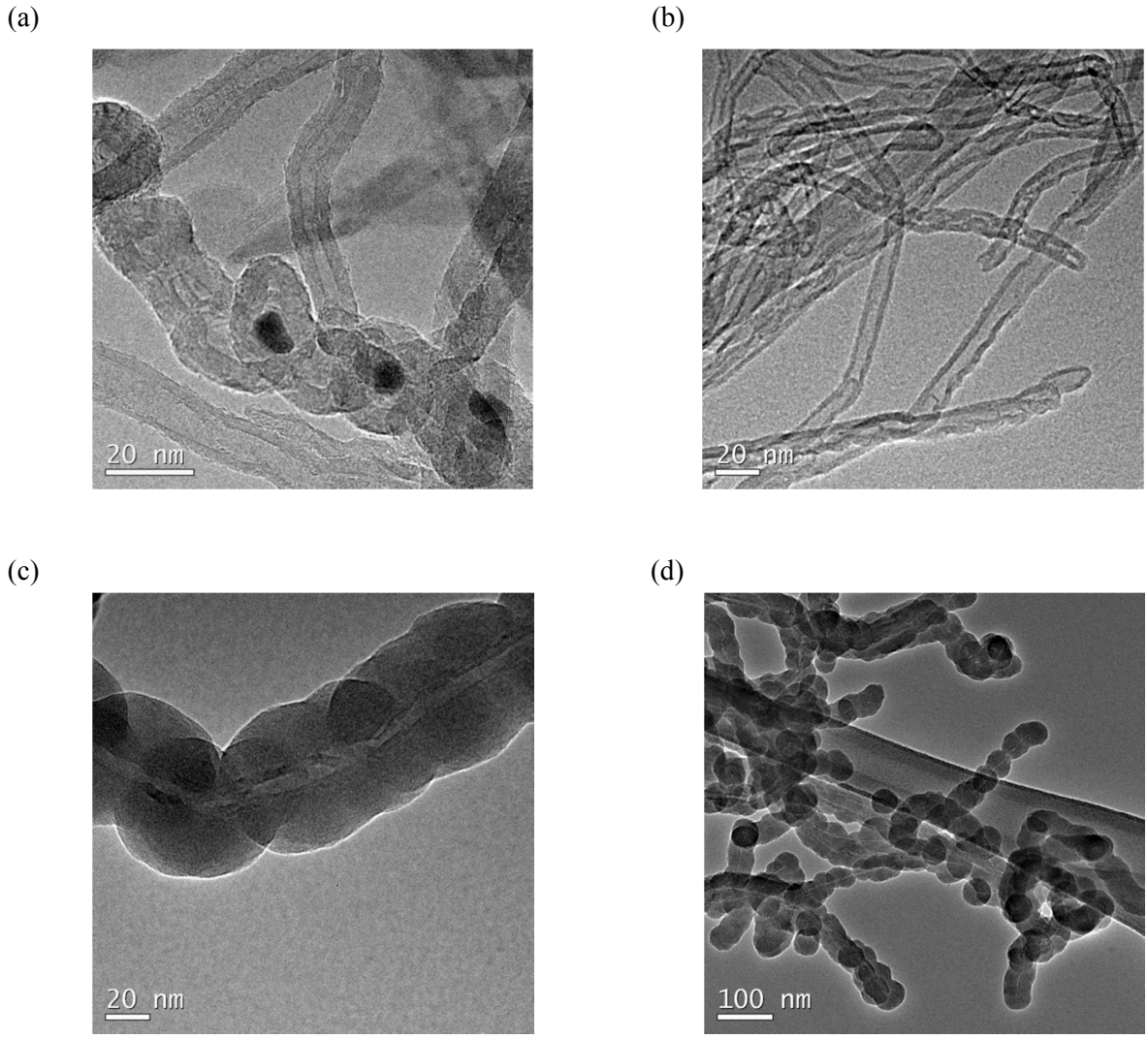

Figure3. 2. (a) is the transmission electron microscope (TEM) image of CNT, (b) is an acid-oxidized MWCNTs (denoted as o-MWCNTs), (c) and (d) are SiO_2 coated CNT.

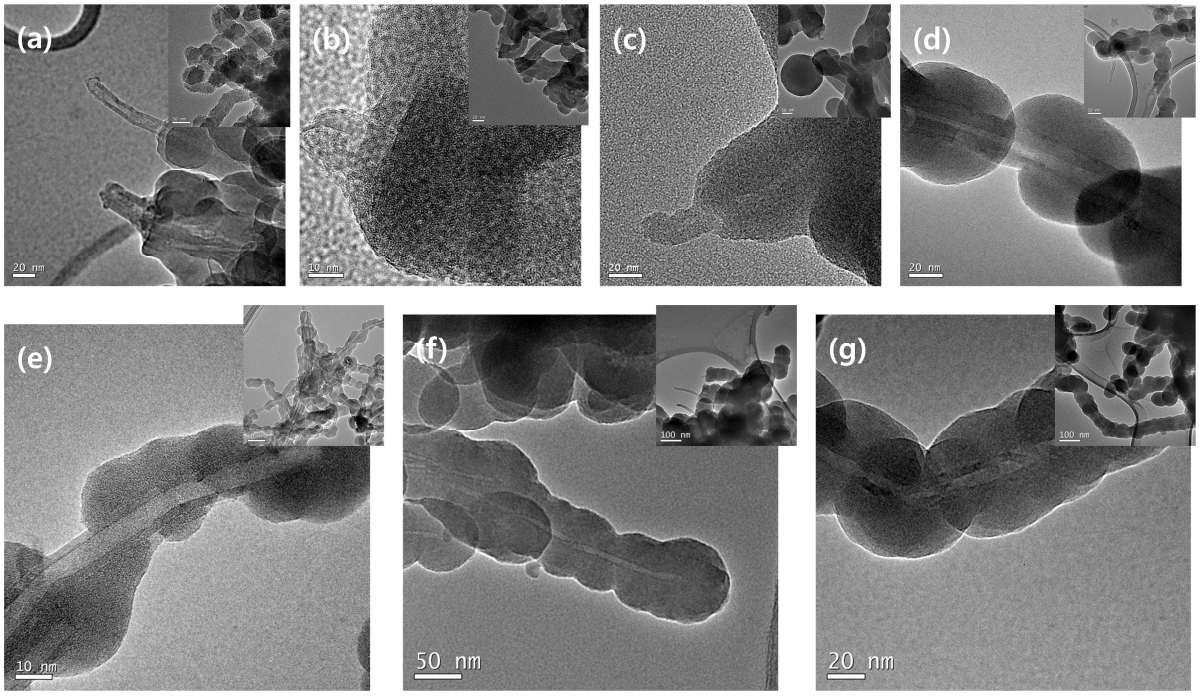

Figure3.3. TEM images of CNT/SiO_2 core/shell structures. The amounts of NH_4OH and silica precursor are 48 mL/16 mL (a), 24 mL/16 mL (b), 12 mL/16 mL (c), 9 mL/16 mL (d), 9 mL/8 mL (e), 12 mL/12 mL (f), 12 mL/ 9 mL(g), respectively. Insets show low magnified TEM images of CNT/SiO_2 structures.

(a)

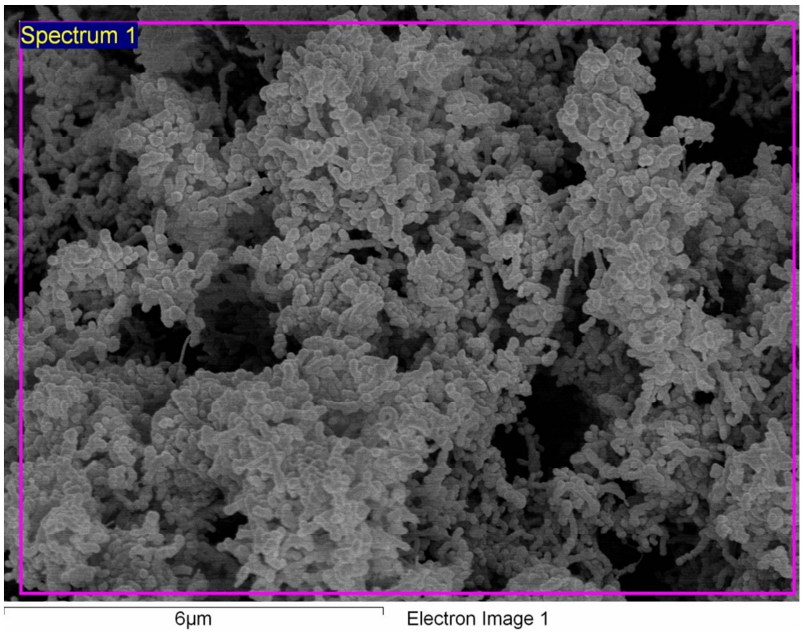

(b)

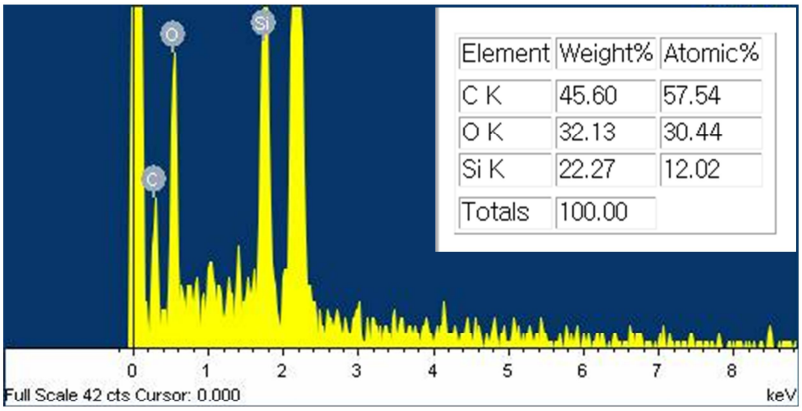

Figure3.4. (a) SEM image of CNT-SiO_2 composite assembled in microscale and (b) its EDAX analysis showing contents of silica coated onto the CNT surface.

Figure3.5 presents an X-ray diffraction (XRD) of CNT/SiC/Si that is prepared from magnesiothermic reduction process of the CNT/SiO_2 composite, in which all XRD peaks are matched with pure Si, indicating successful conversion of the SiO_2 to Si. The magnesiothermic reduction process was processed as following: $SiO_2 + 2Mg = 2MgO + Si$ (1)

Also, the reaction may involve formation of Mg_2Si in the early stages (Eq. 2), followed by reduction of SiO_2 by Mg_2Si through the following chemical reactions (Eq. 3):

$$SiO_2(s) + 4Mg(g) = 2MgO(s) + Mg_2Si(s)\ \Delta G°(900°C) = -308.5\ kJ/mol\ (2)$$

$$Mg_2Si(s) + SiO_2(s) = 2MgO(s) + 2Si(s)\ \Delta G°(900°C) = -181.8\ kJ/mol\ (3)$$

In the presence of excess Mg in the reactants, more Mg_2Si may form by consuming elemental silicon through the reaction: $Si(s) + 2Mg(g) = Mg_2Si(s)\ \Delta G°(900°C) = -63.4\ kJ/mol$ (4)

Above chemical equations tell us that we should match the molar ratio between Mg and SiO_2 to obtain pure Si. Bao et al. reported conversion of diatom frustules (SiO_2) to porous nanocrystalline silicon using Mg vapor at 650°C which is the melting point of Mg. In this case, reduction reaction occurred from the surface to the interior of silica particles and yields the mixture of MgO and Si. Relatively low reduction temperature at 650 °C and formation of MgO phases intertwined with the silicon product inhibited substantial coarsening and sintering of the silicon product.[41] However, magnesiothermic method has not found wide industrial application since the exothermic reactions cause excessive temperatures and result in forming magnesium silicide (Mg_2Si) with Si product. [42] The formation of Mg_2Si is affected by the excess Mg and reduction temperature. Decreasing magnesium amount resulted in decreasing Mg_2Si and with increasing temperatures at fixed ratio of Mg to SiO_2, the formation of Mg_2Si increased.[43] However, in this study by Kalem[43], Mg_2SiO_4 under certain conditions was not taken into account. In addition, quantitative study of phases of the reduction products was not performed and assessment of phases was solely based on intensity of Mg_2Si, MgO and Si peaks. For this reason, the exact effect of reduction conditions on the formation of phases was not well established. Several intermediate steps may be involved with most of the gas-solid reaction systems.[43, 34]

In our study, the magnesiothermic reduction process of the CNT/SiO_2 produced small amount of SiC including Si. The SiC composites are not good for electrochemical performance, since the SiC reacts with lithium ion, but the lithium ions in the lithiated products are not delithiated.[44] To prevent the formation of the SiC layer, we used another strategy to synthesize CNT/TiC/Si composites. Before entering SiO_2 layer on the CNT, TiO_2 layer was conformally coated on the CNT surface. When 1 mL of TB was added into ethanol/EG solution containing 0.2 g oxidized CNTs, the amorphous TiO_2 layer having 5~10 nm thickness was conformally coated on the CNT surface (Figure 3.6a)

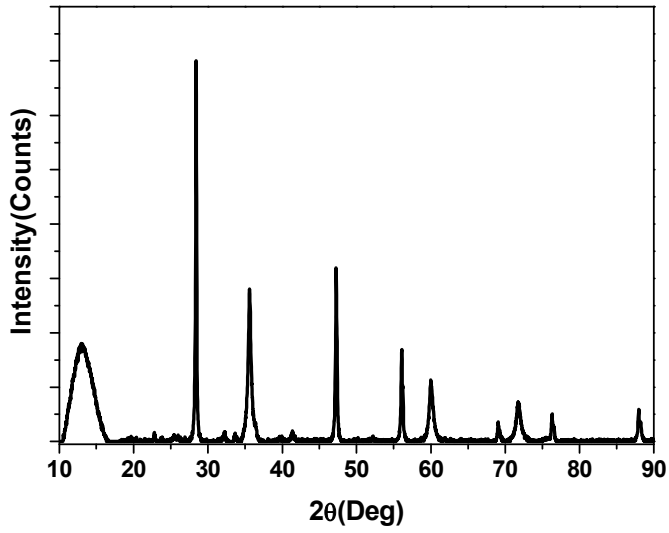

Figure3.5. X-ray Diffractometer image of CNT-SiC-Si

(a) (b)

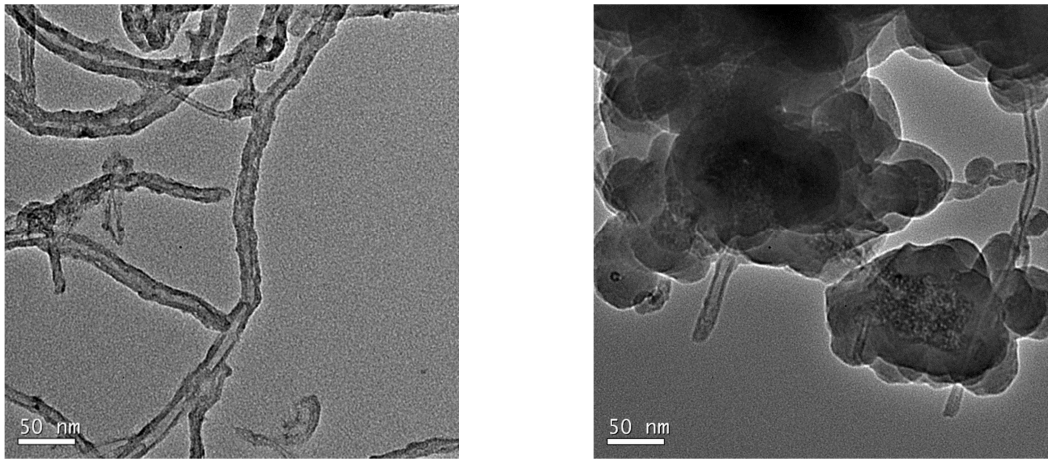

Figure3. 6. TEM images of (a) TiO_2 coated CNT and (b) SiO_2 coated CNT/TiO_2 structure.

Subsequently, SiO_2 layers were coated on the CNT/TiO_2 surface to make CNT/TiO_2/SiO_2 (Figure 3.6b). Similar to the CNT/SiO_2 micro-/nanostructure, the CNT/TiO_2/SiO_2 was assembled in micro-/nanoscale (Figure 3.7a). From the EDAX analysis, 32 wt% silica and 1.5 wt% titania contents were detected (Figure 3.7b). Depending on the amount of silica and titania precursor, the thickness of SiO_2 and TiO_2 shell can be tuned. When the CNT/TiO_2/SiO_2 sample was reacted with Mg vapor at 700 ^oC for 1 h, and followed by rinsing with 1 M HCl, the CNT/TiC/Si composites may be formed due to the reaction sequence of Mg vapor. Under the thermodynamic condition of SiO_2 and TiO_2, TiO_2 layer may react with Mg vapor at 700 ^oC before the SiO_2.[45]

The XRD patterns of as-synthesized CNT/TiC/Si showed complicated peaks including TiC, Mg_2Si and Si. Since the TiC layer is well-known to high electrical conductive materials, this composite anode material may exhibit better electrochemical performance than the CNT/SiC/Si composite.

Before the cell test of the composite anode materials, the electrochemical properties of pristine CNT were carried out. The first discharge and charge capacity of bare CNT at a 0.1 C rate are 900 and 200mAh /g, corresponding to a coulombic efficiency of 22.2% (Figure 3.9a). The cycling performance showed that a low capacity of <150 mAh/g was exhibited (Figure 3.9b). In contrast, when the Si layer was introduced as the CNT/SiC/Si composite, the electrochemical test of the composite anode was carried out at a 0.1 C rate in the range of 0.01 V to 1.2 V. The first discharge and charge capacity of at a 0.1 C rate are 715 and 1060mAh/g, corresponding to a coulombic efficiency of 67.4%. It's discharge capacity of 715mAh/g is much better than the bare CNT (Figure 3.10a). However, poor cycling performance was seen due to a formation of unstable SEI layer (530 mAh/g after 50 cycles) (Figure 3.10b). Therefore, we carried out additional carbon coating by thermal decomposition of acetylene gas at 800 ^oC.

The electrochemical performances of the CNT/SiC/Si with additional carbon layer were shown in Figure 3.11. The first charge capacity of the CNT/SiC/Si at a 0.1C rate is 1183 mAh/g. And, the remarkably enhanced cycling performance was seen (negligible capacity loss after 50 cycles) (Figure 3.11b). Even though the cycling performance is very good, the coulombic efficiency in the first cycle is worse due to the increasing amount of SiC during carbon coating.

(a)

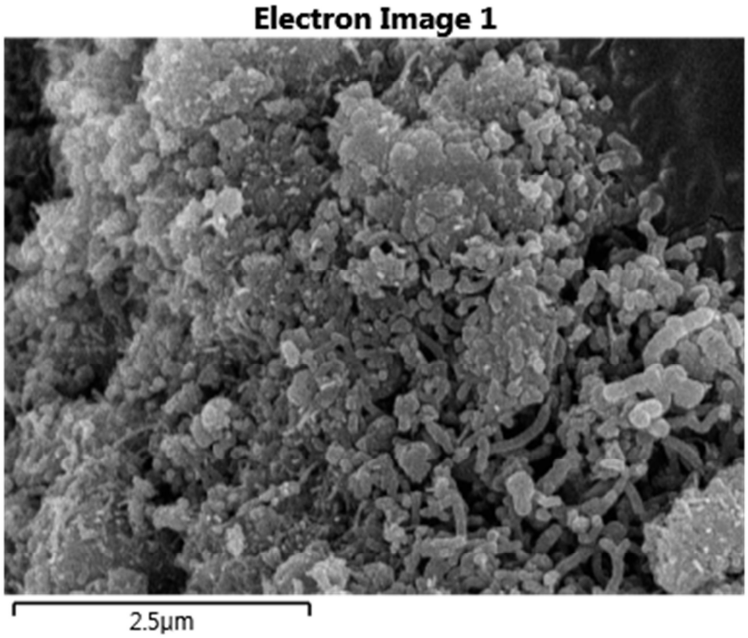

(b)

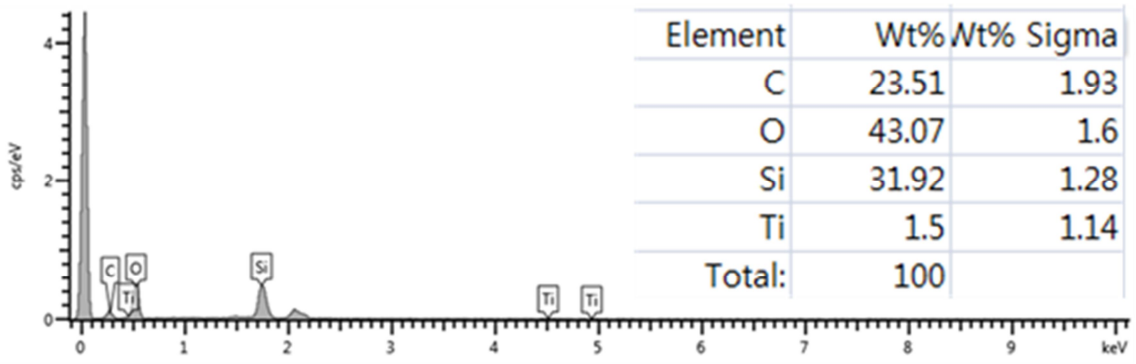

Element	Wt%	Wt% Sigma
C	23.51	1.93
O	43.07	1.6
Si	31.92	1.28
Ti	1.5	1.14
Total:	100	

Figure3.7. (a) presents a Scanning Electron Microscope(SEM) image of CNT/TiO_2/SiO_2 and (b) is showing that EDAX analysis of contents of titania &silica shell

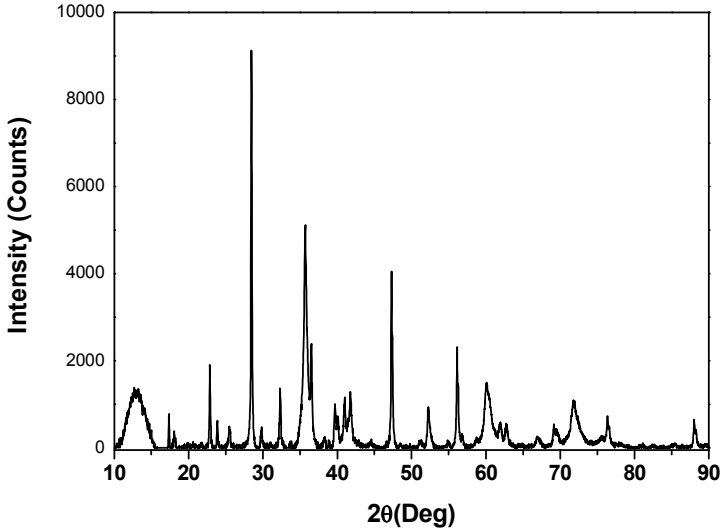

Figure3.8. XRD pattern of CNT/TiC/Si. The XRD patterns show Si, Mg_2Si, and TiC peaks

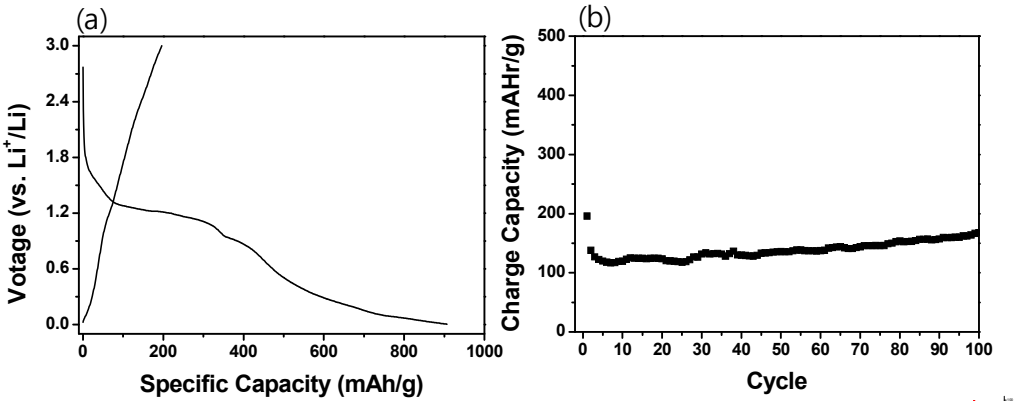

Figure3.9. The electrochemical performance of bare CNT: (a) charge and discharge profile of the bare CNT, (b) cycling life of the bare CNT.

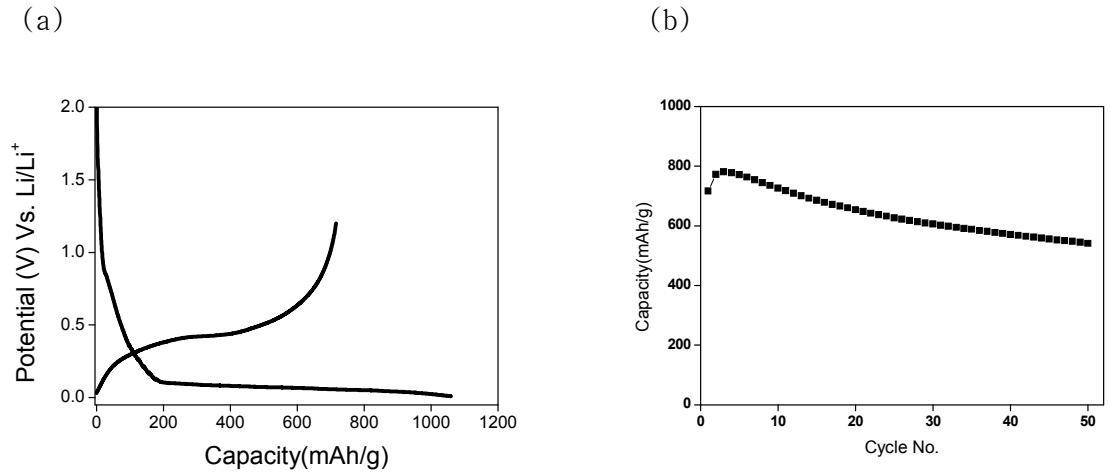

Figure3.10. The electrochemical performance of the as-synthesized CNT/SiC/Si composites: (a) charge and discharge profile of CNT/SiC/Si composites, (b) cycling life of CNT/SiC/Si composites.

(a) (b)

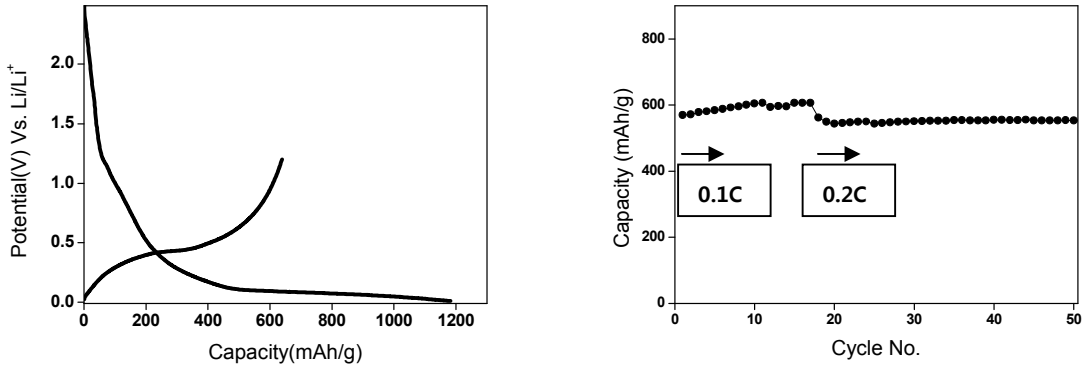

Figure3.11. The electrochemical performance of the CNT/SiC/Si composites with additional carbon layer: (a) charge and discharge profile of CNT/SiC/Si-C composites, (b) cycling life of CNT/SiC/Si-C composites.

(a) (b)

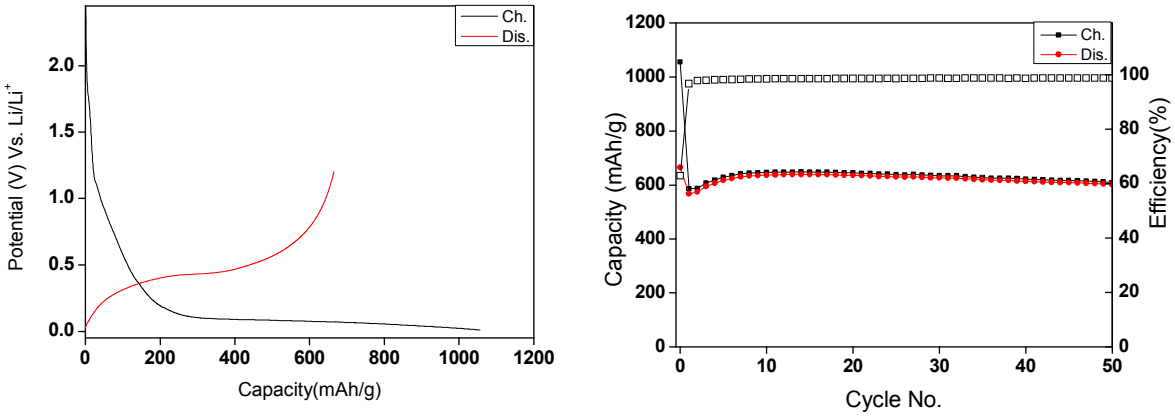

Figure3.12. The electrochemical performance of the CNT/TiC/Si composites with additional carbon layer: (a) charge and discharge profile of CNT/TiC/Si-C composites, (b) cycling life of CNT/TiC/Si-C composites.

To solve this problem, we prepared the CNT/TiC/Si composite anode. Figure 3.12(a) presents the electrochemical performance of the CNT/TiC/Si with additional carbon layer. The first discharging capacity of the composites at a 0.1C rate is 1056 mAh/g with an increased coulombic efficiency of 62.9 %. The introduction of TiC layer may reduce side reaction that occurred in the SiC, resulting in an enhanced coulombic efficiency in the first cycle. Also, the good cycling performance was observed after 50 cycles (capacity loss of <10%).

4. Conclusion

In summary, we successfully synthesized CNT/Si composites via magnesiothermic reduction process of CNT/SiO_2 and CNT/TiO_2/SiO_2. The SiO_2 and/or TiO_2 sol precursors have been successfully coated onto the oxidized CNT surface. The proposed methodology has several advantages in that the thickness and architectures of SiO_2 or TiO_2 coating can be easily controlled by rationally adjusting reaction parameters such as precursor or catalyst concentration, as well as addition of structure-directing agents. And subsequent heat treatment led to removal of water and stable SiO_2 or TiO_2 shell structure. Finally, magnesiothermic reduction process led to a formation of CNT/SiC/Si or CNT/TiC/Si composites. Since the CNTs core are electrically conductive and Si shell can exhibit a high specific capacity, CNT/Si composite electrodes exhibit high electrochemical performances, including a high specific capacity and an excellent rate capability. This process opens up a way to make other Si composites anode materials for high performance lithium-ion batteries.

5. References

[1] M. Mohri, N. Yanagisawa, Y. Tajima, H. Tanaka, T. Mitate, S. Nakajima, M. Yoshida, Y. Yoshimoto, T. Suzuki, H. Wada. *J. Power Sources* **1989**, *26*, 545-551

[2]Y. P. Wu, C. Jiang, C. Wan, R. Holze. *Electrochem. Commun.* **2002**, *4*, 483-487

[3] Y. P. Wu, E. Rahm, R. Holze. *J. Power Sources* **2003**, *114*, 228-236.

[4]K. Sato, M. Noguchi, A. Demachi, N. Oki, M. Endo. *Science* **1994**, *264*, 556-558.

[5] S. Yata, Y. Hato, H. Kinoshita, N. Ando, A. Anekawa, T. Hashimoto, M. Yamaguchi, K. Tanaka, T. Yamabe. *Synth. Met.* **1995** *,73*, 273-277.

[6] Y. P. Wu, S. B. Fang, Y. Y. Jiang. *J. Mater. Chem.* **1998***, 8*, 2223-2227.

[7] Y. P. Wu, S. B. Fang, Y. Y. Jiang. *Solid State Ionics* **1999**, *120*, 117-123.

[8] Y. P. Wu, S. B. Fang, Y. Y. Jiang. *J. Power Sources* **1998***, 75*, 201-206

[9] Y. Idota, T. Kubota, A. Matsufuji, Y. Maekawa, T. Miyasaka. *Science* **1997***, 276*, 1395-1397.

[10] D. L. Foster, J. Wolfensine, J. R. Read, W. K. Behl. *Electrochem. Solid-State Lett*. **2000**, *3*, 203-204.

[11] N. C. Li, C. R. Martin, B. Scrosati. *Electrochem. Solid-State Lett*. **2000**,*3*, 316-318.

[12] Y. Wang, J. Y. Lee. *J. Phys. Chem. B* **2004***,108*, 17832-17837.

[13] Y. Liu, T. Matsumura, N. Imanishi, T. Ichikawa, A. Hirano, Y. Takeda. *Electrochem. Commun.* **2004** *,6*, 632-636.

[14] D. Souza, V. Pralong, A. J. Jacobson, L. F. Nazar. *Science* **2002***,296*, 2012-2015.

[15] H. Pfeier, F. Tancret, M. P. Bichat, L. Monconduit, F. Favier, T. Brousse. *Electrochem. Commun.* **2004***, 6*, 263-267

[16] B. Laik, P. Poizot, J. M. Tarascon. *J. Electrochem. Soc.* **2002** *,149*, A251-A255.

[17] D. Larcher, G. Sudant, J. B. Leriche, Y. Chabre, J. M. Tarascon. *J. Electrochem. Soc.* **2002**,*149*, A234-A241.

[18] Y. M. Kang, K. T . Kim, J. H. Kim, H. S. Kim, P. S. Lee, J. Y . Lee, H. K. Liu, S. X. Dou. *J. Power Sources* **2004***,133*, 252 -259.

[19] Y. P. Wu, X. B. Dai, J. Q. Ma, Y. J. Chen. *Lithium Ion Batteries: Practice and Applications*, Chemical Industry Press, Beijing (2004).

[20] J. Rowsell, V. Pralong, L. Nazar. *J. Am. Chem. Soc.* **2001***,123*, 8598-8599

[21] N. Perira, L. Duppont, J. M. Trarscon, L. C. Klein, G. G. Amatucci. *J. Electrochem. Soc.* 2003*,150*, A1272

[22] H. Jun, M. Park, Y. Yoon, G. Kim, S. Joo. *J. Power Sources* 2003*,115*, 346-351

[23] T. Matsumura, N. Sonoyama, R. Kanno, M. Takano. *Solid State Ionics* **2003***,158*, 253- 260

[24] L. J. Fu, H. Liu, Y. P. Wu, E. Rahm, R. Holze, H. Q. Wu. *Prog. Mater. Sci*. **2005**, *50*, 881-928.

[25] Y. P. Wu, E. Rahm, R. Holze. *Electrochim. Acta* **2002**,*47*, 3491- 3507

[26] P. Polzot, S. Laruelle, S. Grugeon, L. Dupont, J. M. Tarascon. *Nature***2000** *,407*, 496-499

[27] H. Kim, J. Choi, H. J. Sohn. *J. Electrochem. Soc.* **1999** ,*146*, 4401-4405

[28] J. Yang, Y. Takeda, N. Imanishi, O. Yamamoto. *J. Electrochem. Soc.* **1999***,146*, 4009- 4013

[29] N. C. Li, C. R. Martin. *J. Electrochem. Soc.* **2001** *,148*, A164- A170

[30] D. S. Wu, C. Y. Han, S. Y. Wang, N. L. Wu, I. A. Rusakova. *Mater. Lett.* **2002** *,53*, 155-159

[31] S. Ohara, J. Suzuki, K. Sekine, T. Takamura. *J. Power Source* **2003** *, 591,*119–121,

[32] T. ZHANG et al.*Pure Appl. Chem.*, **2006**, *78* ,1889–1896.

[33] Q. Wang et al. *Carbon* **2001** *,39* , 2211 –2214

[34] Sarder Elius Sadique, Production and Purification of Silicon by Magnesiothermic Reduction of Silica Fume (2010) pp. 11

[35] J. O. Bensenhard, J. Yang, M. Winter. *J. Power Sources* **1997** *,68*, 87- 90.

[36] H. Li, X. Huang, L. Chen. *Solid State Ionics* **2000**, *135*, 181-191

[37] Y. Zhang, Z. W. Fu, Q. Z. Qin. *Electrochem. Commun.* **2004***, 6*, 484-491

[38] T. Moritaz, N. Takami. *J. Electrochem. Soc.* **2006** *, 153*, A425-A430

[39] Y. Liu, K. Hanai, T. Matsumura, N. Imanishi, A. Hirano, Y. Takeda. *Electrochem. Solid-State Lett.* **2004***,7*, A492-A495

[40] Y. P. Wu, C. R. Wan, C. Y. Jiang, S. B. Fang. *Lithium Secondary Ion Batteries*, Chemical Industry Press, Beijing (**2002**).

[41] Z. Bao, M.R. Weatherspoon, S. Shian, Ye Cai1, P.D. Graham, S.M. Allan, G. Ahmad, M.B. Dickerson, B.C.Church, Z. Kang, H.W. Abernathy, C.J. Summers, M. Liu, K.H. Sandhage. Nature, **2007**,*446*, 172-175.

[42] N.H. Zulumyan, A.R. Isahakyan, Z.H. Hovhannisyan , A.R. Torosyan: *The influence of mechanical activation on the process of thermal reduction of silica by magnesium powder.* A.A. Luo, N.R. Neelameggham, R.S. Beals :USA, 2006; pp 351-354.

[43] T. Kalem; *Gas-solid displacement reactions for converting silica diatom frustules into MgO and TiO2*. Iowa State University (Master's Thesis): USA 2004.

[44] Albert L. Lipson, Sudeshna Chattopadhyay, Hunter J. Karmel, Timothy T. Fister, Jonathan D. Emery, Vinayak P. Dravid, Michael M. Thackeray, Paul A. Fenter, Michael J. Bedzyk, Mark C. Hersam,*J. Phys. Chem. C* **2012**, *116*, 20949−20957

[45] Youn-Bae Kang, In-Ho Jung, Hae-Geon Lee, *Computer Coupling of Phase Diagrams and Thermochemistry* **2006,** *30***,** 226–234

Part 3: High-Performance Si Anodes with Highly Conductive and Thermally Stable Titanium Silicide Coating Layer

1. Introduction

Rechargeable lithium-ion batteries (LIBs) have been developed as the most promising power source technology for portable electronics (e.g., cell phones, laptop computers, digital cameras, etc.) and vehicles (e.g., hybrid vehicle, electric vehicle, etc.).[1,2] In the last decade, substantial efforts have been devoted to the replacement of conventional carbon-based anode materials in LIBs with alternatives that allow a high energy density.[3-5]

Silicon is an attractive anode material for next-generation LIBs owing to its abundant availability, its low discharge potential (<0.4 V vs. Li/Li^+) and high theoretical gravimetric capacity (3579 mAh g^{-1} at room temperature).[6-8] However, the practical use of Si anode material in LIBs is hindered by its poor cyclability resulting from the low intrinsic electric conductivity and the huge volume change (>300%).[9,10]The use of nanostructured materials is an effective approach to solve this issue. Nanostructured Si anode materials, including nanoparticles, nanowires, nanotubes, hollow spheres, and porous structures, showed significantly improved cycle performances by accommodating the large volume change.[4,11-18]

An alternative approach for improving the stability of Si is to use surface coating. The surface of an electrode material can greatly influence the electrochemical properties. Since the electrochemical potential of Si alloying is below the solvent reduction level, it leads to the formation of unstable solid electrolyte interface (SEI) layers, including an abundant amount of fluorinated carbon and Si species. [19] During lithium insertion/extraction process, the SEI layers become thicker, resulting in the degradation in electrochemical performance.[19, 20] Therefore, a uniform and compact SEI layer on the electrode surface may enhance the efficiency and cycling stability of the electrode. Typically, carbon-based materials, metal particles, metal oxide particles, and conductive polymers have been used as coating materials to enhance the electrical conductivity of Si and to form a stable SEI layer, resulting in improved electrochemical performances.[18, 21-33]

As another simple method, a silicothermic reduction process can provide an attractive means to coat titanium silicide (Ti_xSi_y) on the surface of Si. Since the Ti_xSi_y is light-weight, highly electrically conductive, and thermally stable, when it is combined with Si particles, significantly improved electrochemical performances can be expected.[34-36] For example, Zhou et al. reported a synthesis of hetero-nanostructures consisting of $TiSi_2$ nanonets and Si nanoparticles via chemical vapor deposition process. The hetero-nanostructured anode materials exhibited remarkable electrochemical performances, including high capacity and long cycling life. However, the amount of inactive $TiSi_2$ should be minimized to make high energy density LIBs.[36]

Herein, we report a simple synthesis of Ti_xSi_y coated Si nanoparticles via a silicothermic reduction process, in which Si acts as the reducing agent, while titanium oxide is used as a source material of Ti. The titanium silicide enhances the electrical conductivity of Si nanoparticles and provides a highly stable SEI layer during the cycling, resulting in superior electrochemical performances including a high reversible capacity (1470 mAh /g) and a high rate capability (1150 mAh /g at 20 C rate). Moreover, the Ti_xSi_y-coated Si electrodes showed significantly improved high thermal stability, compared to bare Si electrodes.

The synthetic approach of Ti_xSi_y-coated Si nanoparticles is briefly described in the schematic illustration of Figure 4.1. We developed a simple wet-chemical synthetic route to conformally coat TiO_2 onto the surface of Si particles by controlled hydrolysis of the titanium precursors. Subsequent two-step annealing processes led to a formation of Ti_xSi_y-coated Si particles. A detailed explanation of the synthetic procedures is given in the experimental section.

2. Experimental

2.1 Materials

Chemical reagents used for the synthesis of Ti_xSi_y-coated Si particles, including Si nanopowder, Titanium tetrabutoxide, Ethylene glycol were purchased from sigma aldrich. Ethanol was obtained from J.T.Baker.

2.2 Preparation of Ti_xSi_y-coated Si particles

Preparation of Ti_xSi_y-coated Si particles: Si nanopowder (Sigma-Aldrich, 50 nm in size) was cleaned in acetone and isopropyl alcohol and dried under nitrogen. In a typical synthesis, a 0.2 mL of titanium tetrabutoxide and 0.2 mL of H_2O were refluxed in ethylene glycol/ethanol (16 mL/4 mL) at 80 ^oC for 6 h in the presence of 1g Si particles. As-synthesized TiO_2-coated Si powders were cleaned with ethanol several times and dried at 80 ^oC for 12 h. Subsequently, the TiO_2-coated Si particles were thermally annealed in a quartz furnace at 450-1000 ^oC for 1 hr under argon stream to make Ti_xSi_y-coated Si particles.

2.3 Measurements and characterization

Characterization of Ti_xSi_y-coated Si particles: The crystal structures of Ti_xSi_y-coated Si sample were measured by high power X-ray diffractometer (XRD) on a Rigaku D/MAX at 2500 V using Ni-filtered Cu Kα radiation. TEM images were taken in the bright-field mode using JEM 1400 (JEOL) operated at 120 kV accelerating voltages.

Thermal analyses of lithiated Ti_xSi_y-coated Si particles: To measure the thermal properties of lithiated Si electrodes with electrolytes, coin cells were charged to 0.005 V vs. Li/Li^+ and then

carefully opened in a dry room. The retrieved electrodes were rinsed in a DMC solvent to remove residual electrolyte and then dried. The resulting lithiated silicon electrode was sealed together with an electrolyte in a hermetic stainless-steel pan (Perkin Elmer). All of the DSC (METTLER TOLEDO DSC 1) measurements were carried out at a heating rate of 5 ^{o}C min^{-1} in a range of 30-400 ^{o}C. The amount of entrapped electrolyte was 50 wt% based on the lithiated silicon material.

Electrochemical performance: Electrochemical cell test was performed using coin-type half cells (2016R type) by assembling in an argon-filled glove box. Ti_xSi_y-coated Si and bare Si electrodes for the cell test were composed of Si active material (70 wt%), super P carbon black (10 wt%), and poly(acrylic acid)/sodium carboxymethyl cellulose (wt/wt, 50/50) binder (20 wt%). The electrolyte was composed of 1.3 M $LiPF_6$ in a mixture of ethylene carbonate/diethylene carbonate (ED/DEC, 30/70 vol.%) with 5 wt% fluoroethylene carbonate (FEC) additive. The cells were cycled at a rate of 0.1-20 C in the range of 0.005 and 1.2 V.

2.4 Result and discussion

Figure 1A presents a transmission electron microscope (TEM) image of Si nanoparticles, showing that the particles consist of a crystalline Si core (ranging from 30 to 100 nm in diameter) and an SiO_2 shell with thickness of ~1 nm (Inset of Figure4.1A). When equal amounts of titanium tetrabutoxide and H_2O were refluxed in a mixture of ethylene glycol/ethanol in the presence of 1g Si particles, the amorphous TiO_2 precursor was conformally coated on the surface of the Si particles with an average thickness of ~10 nm (Inset of Figure4.1B). The Ti amount of 2.4 wt% was confirmed by inductively coupled plasma mass spectrometry (ICP) analysis. With an increasing Ti precursor, the Ti contents in the final products were linearly increased (see Supporting Information (SI), Fig. S1). The TiO_2 coated Si particles were subsequently annealed at 450 ^{o}C for 1 h to prepare TiO_2-decorated Si powders. Consequently, amorphous TiO_2 were transformed to crystalline TiO_2 having an average particle size of 5 nm (Figure 1C). As the TiO_2-decorated Si particles were further annealed at 1000 ^{o}C for 1 h in argon, the TiO_2 was transformed to Ti_xSi_y via a silicothermic reduction process, as will be discussed later (Figure4.1D).

Figure 4.2.To investigate the formation mechanism of Ti_xSi_y-coated Si particles, we obtained X-ray diffraction (XRD) patterns and X-ray photoelectron spectroscopy (XPS) results. XRD patterns of TiO_2-decorated Si annealed at 450 ^{o}C showed that crystalline Si peaks were clearly observed (black line in Figure4.2A), while a weak peak of crystalline $TiSi_2$ phase was detected at 42^{o}, as indicated in the inset of Figure 2A. When the annealing temperature was increased to 1000 ^{o}C, the intensity of the $TiSi_2$ peak was significantly increased (solid circle in the inset) and a new phase of Ti_5Si_3 (solid star) and Ti_5Si_4 (solid triangle) was developed, (the inset of Figure4.2A). The Ti_5Si_3 and Ti_5Si_4 phases were formed as the $TiSi_2$ phase was further reacted with additional Ti, as marked in the Ti-Si binary phase

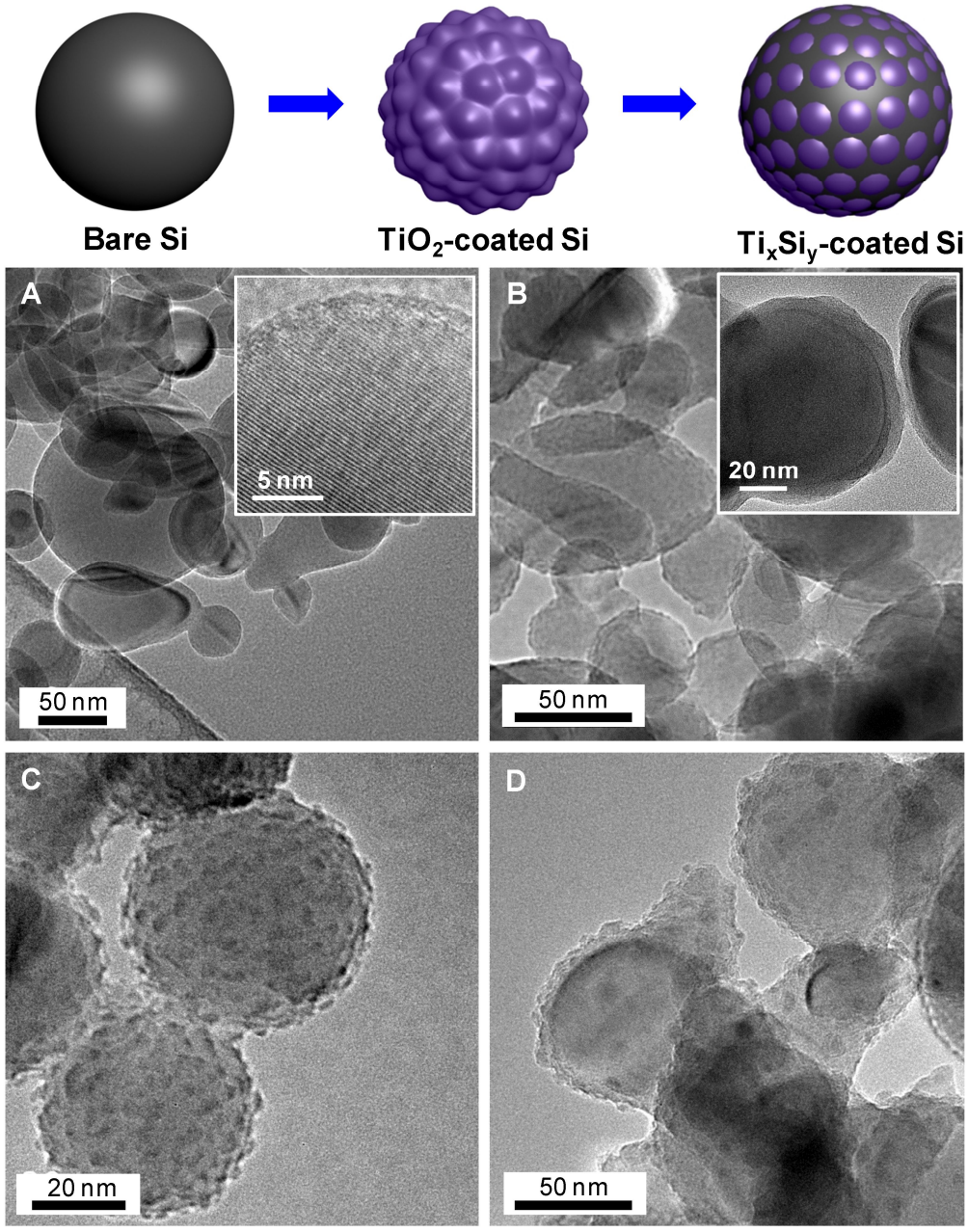

Figure4. 1. Synthesis of Ti_xSi_y-coated Si nanoparticles. Top: Schematic illustration preparing Ti_xSi_y layer on the surface of Si particles. Bottom: (A) TEM image of bare Si particles and magnified TEM image (inset of panel A) showing crystalline Si core and SiO_2 shell, (B) TEM image of TiO_2-coated Si particles and magnified image (inset of panel B) showing thickness of TiO_2 layer, (C) TEM image of TiO_2-coated Si particles annealed at 450 ^oC, and (D) TEM image of Ti_xSi_y-coated Si particles obtained by annealing at 1000 ^oC.

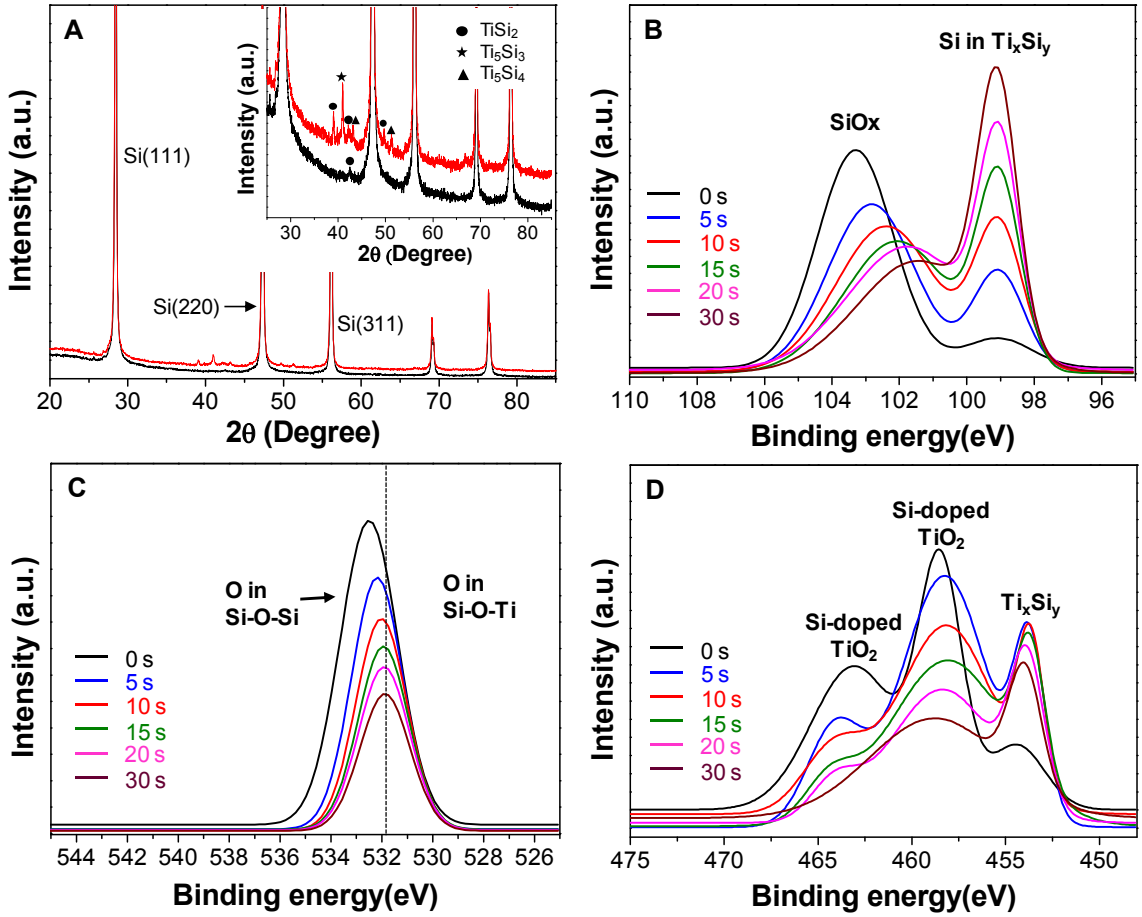

Figure4. 2. Characterization of Ti_xSi_y-coated Si nanoparticles. (A) XRD patterns show Ti_xSi_y-coated Si particles annealed at 450 ^oC (black line) and 1000 ^oC (red line). In the inset, $TiSi_2$, Ti_5Si_3, and Ti_5Si_4 phases were clearly observed. (B) XPS spectra of Si 2p core level shows existence of Ti_xSi_y layer and a formation of Ti-O-Si. XPS depth profiling data indicates successful synthesis of Ti_xSi_y layers on the surface of Si particles. XPS spectra of (C) O 1s and (D) Ti 2p core level confirm the formation of strong bonding between Si and TiO_2 (Ti-O-Si) and Ti_xSi_y phase diagram.[37]

In order to characterize the oxidation states of silicon ions, oxygen ions, and titanium ions, XPS spectra of titanium-silicide coated Si samples were obtained. The structures of the coating layers were investigated through the depth profiling by argon ion. The binding energies of Si 2p appearing at 99 eV represent silicon species in the Ti_xSi_y, indicating that Ti_xSi_y-coated Si is successfully synthesized (Figure 4.2B). Also, based on the XPS spectra ranging from 103.5 to 101 eV, pure SiO_x exists in the outermost shell and Ti-associated SiO_x in the inner layers was detected with a short time etching, implying that Si-O-Ti bonds may be formed (Fig. 2B).[38] From the binding energy of O 1s appearing at 533 eV (Si-O-Si) and 532 eV (Si-O-Ti), the formation of Si-O-Ti was confirmed, revealing the strong interaction between TiO_2 and Si (Figure4.2C).[39] The XPS spectra of the Ti 2p core level reconfirmed the formation of Si-doped TiO_2 and Ti_xSi_y. In the outermost shell regions, the peaks appearing at 458.5 and 464.3 eV correspond to the core level of Ti 2p of TiO_2. Ti 2p peaks corresponding to the Si-dope TiO_2 and the Ti_xSi_y were gradually increased through deep depth profiling (Figure4.2D).[40]

The formation of Ti_xSi_y layers can be described as follows: (i) When the TiO_2 coating layers were heated to >900 ^oC, the dissociation of TiO_2 is fast, leaving oxygen vacancies;[41] (ii) At the same temperature, Si atoms easily diffuse into the dissociated and remaining TiO_2 layers to make $TiSi_2$ layers; (iii) The little remaining oxygen may react with the Si to make SiO at the shell regions, in which the SiO will be evaporated at >900 ^oC; (iv) Finally, the Ti_5Si_3 and Ti_5Si_4 phases are formed by the reaction of the preformed $TiSi_2$ phase and additional dissociated Ti. The overall reaction to form Ti_xSi_y is denoted in the following equations: [42]

$$Ti + 2Si \rightarrow TiSi_2 \quad (1)$$

$$TiO_2 + 4Si \rightarrow TiSi_2 + 2SiO\uparrow (>900\ ^oC) \quad (2)$$

$$yTiSi_2 + (2x-y)Ti \rightarrow 2Ti_xSi_y \quad (3)$$

Fig.3 The electrochemical performance of the Ti_xSi_y-coated Si particles (Ti contents of 2.3 wt%) as the anodes in LIBs was tested by galvanostatic discharging and charging at a 0.1-20 C rate in the range of 0.005 V to 1.2 V. The first discharge and charge capacity of bare Si at a 0.1 C rate are 1950 and 1550 mAh g^{-1}, corresponding to a coulombic efficiency of 79.4% (Figure4.3A). Whereas, the first charge capacity of the Ti_xSi_y-coated Si at a 0.1C rate is 1470 mAh g^{-1} with an increased coulombic efficiency of 83.5% (Figure4.3B). The enhanced coulombic efficiency of the first cycle may be due to the uniform Ti_xSi_y coating layer, which can promote the formation of a stable SEI layer on the surface of the Si particles, and reduce the direct contact between Si and the electrolyte.

When the Ti_xSi_y-coated Si electrode was cycled to 90 cycles at a rate of 0.2 C (lithiation) and 0.5 C (delithiation), a high reversible capacity of 1430 mAh g^{-1} was exhibited, corresponding to the capacity retention of >99% (compared to initial capacity) (Figure4.3C). In contrast, the bare Si

electrode showed a fast capacity fading with capacity retention of 51% after 70 cycles (Figure4.3C). It is attributed to poor electrical conductivity and formation of unstable SEI layer.[7] After 30 cycles, TEM image of bare Si showed the porous regions due to a large volume change during cycling, while the morphology of Ti_xSi_y-coated Si was similar to that of the original Si and the inactive Ti_xSi_y layers were still strongly anchored to the Si surface (SI, Fig. S2).

Moreover, rate capabilities of both electrodes were investigated at various C rates (0.2 - 20 C rate) between 1.2 V and 0.005 V with a fixed discharging rate of 0.2 C. The bare Si electrodes exhibited the capacity retention of 66.7% at a high rate of 10 C, compared to that of the 0.2 C rate (Figure4.3D). In contrast, the Ti_xSi_y-coated Si electrode showed significantly enhanced rate capabilities. Even at a high rate of 20 C, the capacity retention of the Ti_xSi_y-coated Si was 87.8% (Figure4.3D). These results suggest that the Ti_xSi_y coating layers play an important role in exhibiting superior electrochemical properties, including highly stable cycling and an excellent rate capability. Since the Ti_xSi_y layers were strongly attached to the Si interface during the silicothermic reduction process, the Ti_xSi_y-coated Si electrodes may exhibit a highly stable cycling. Moreover, the electrical conductivity of the electrodes prepared with the bare Si was 1.87×10^{-4} S/cm, while the Ti_xSi_y-coated Si electrode showed a significant improvement (4.23×10^{-5} S/cm), indicating that the Ti_xSi_y layer served as the effective path for electrical conduction.

To prove the stable cycling of Ti_xSi_y-coated Si electrodes, the XPS spectra were obtained before and after cycling. Interestingly, Li-based SEI layers did not discernibly change between the 1st and 40th cycles, supporting good capacity retention of the Si anodes with the Ti_xSi_y coating layer (SI, Fig. S3).

Figure4.4 In addition, the effect of the Ti_xSi_y coating on the thermal properties of fully lithiated Si electrode was investigated by differential scanning calorimetry (DSC). Heating of fully lithiated bare Si electrode resulted in distinct and sharp exothermic peaks at around 107, 187, 251, and 262 ^oC (Top in Figure 4.4A). It is reasonable that the first exothermic peaks at 100-130^oC correspond to thermal decomposition of metastable SEI components.[43] A DSC heating curve for fully lithiated bare Si shows very large exothermic peaks at 150-320 ^oC, while the presence of the Ti_xSi_y coating layer on fully lithiated Si gives broad exothermic peaks with significantly reduced heat (Bottom in Figure4.4A). It indicates that the Ti_xSi_y coating layer effectually mitigated various exothermic reactions caused by the thermal decomposition reactions of an electrolyte with lithiated Si at elevated temperatures, as depicted in Figure 4.4B. When a cell is heated above a certain temperature, exothermic reactions between the electrodes and the electrolyte take place and lead to an increase of the cell internal temperature. If the generated heat is greater than the energy that can be dissipated, the cell temperature will increase rapidly. This temperature growth will accelerate chemical reactions and lead to the production of even more heat, eventually resulting in the thermal runaway of batteries. From

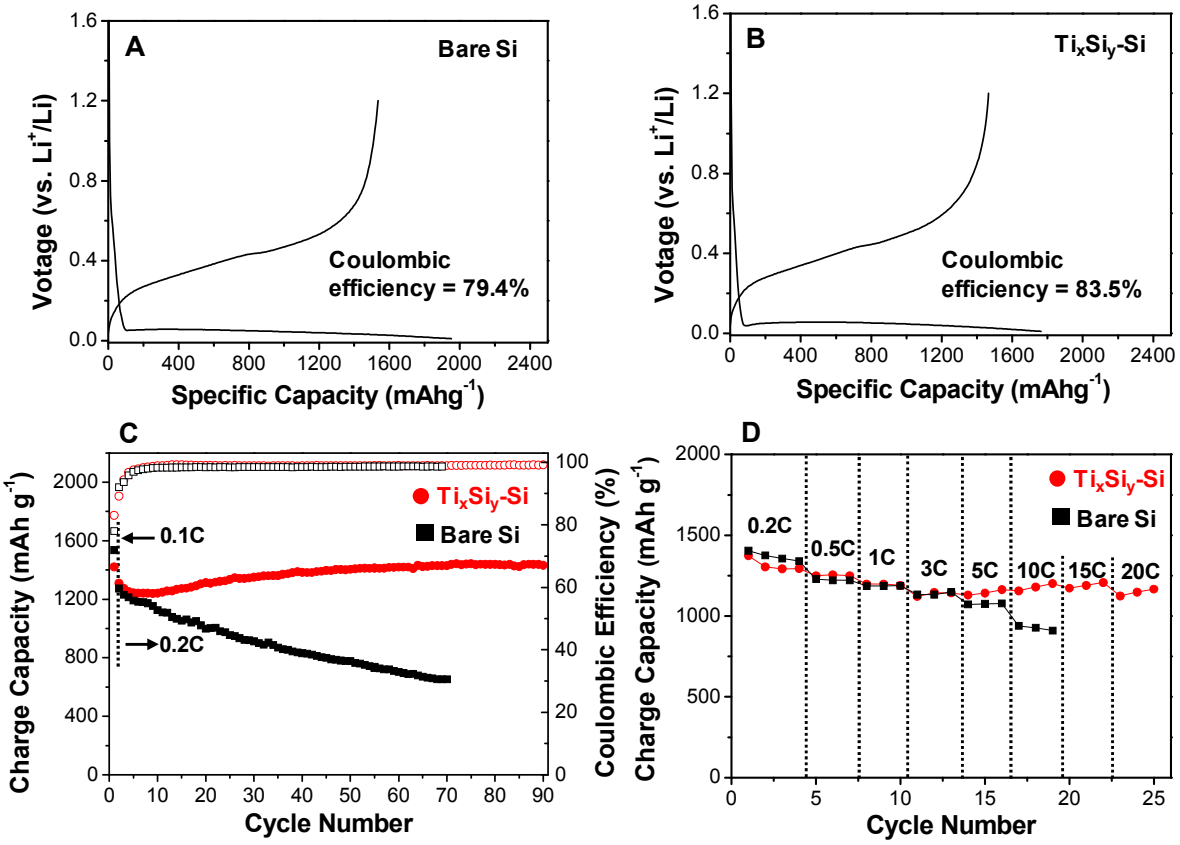

Figure4. 3. Electrochemical performances of Ti_xSi_y-coated Si and bare Si anodes. First cycle voltage profiles of (A) bare Si and (B) Ti_xSi_y-coated Si are obtained at 0.1 C (1st cycle) in the range of 0.005 - 1.2 V. (C) Cycling performances of both electrodes are obtained at 0.1 C (first cycle) and 0.2 C (from second cycle). (D) Rate capabilities of Ti_xSi_y-coated Si (solid circle) and bare Si (solid square) were obtained at 0.2C – 20 C rates.

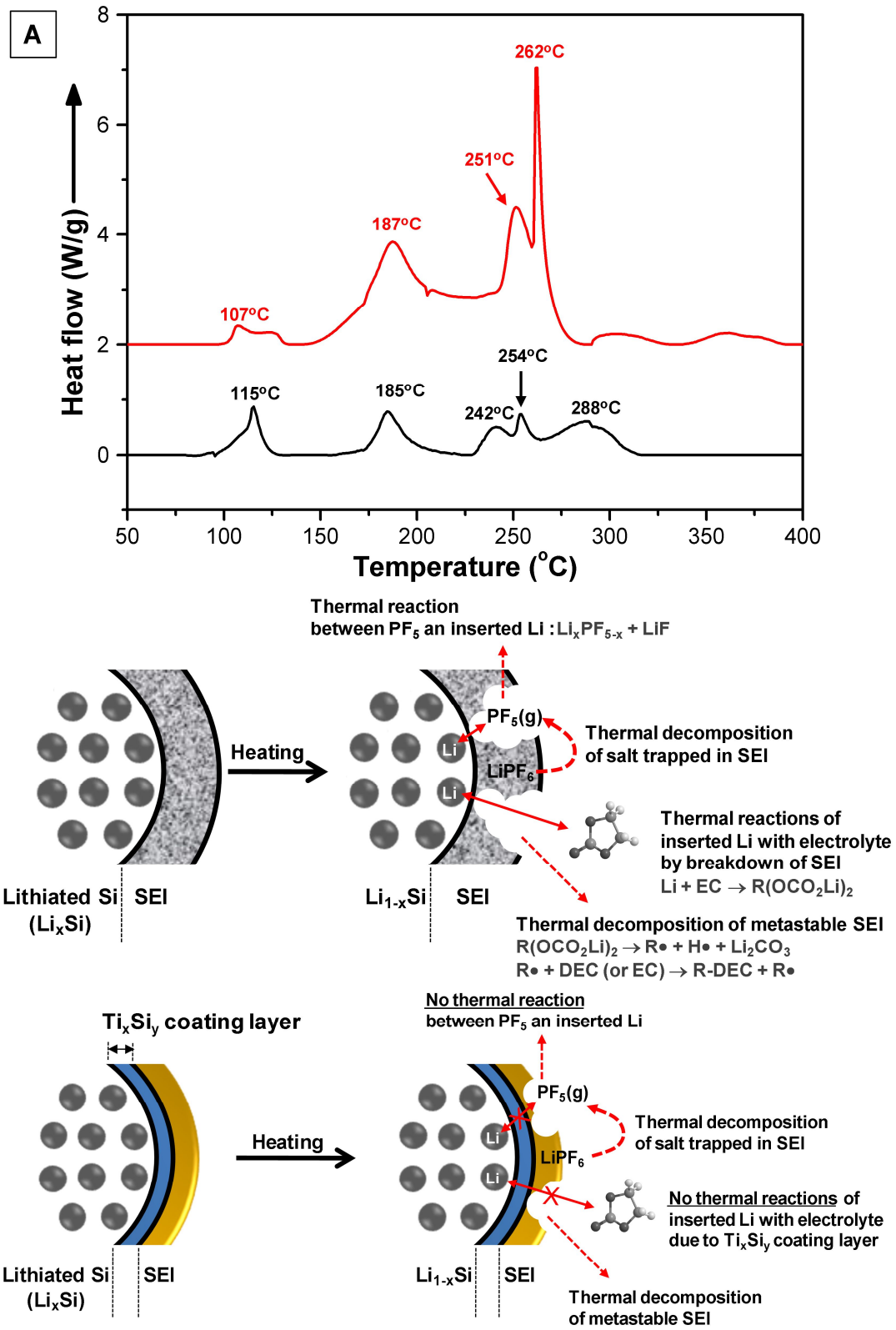

Figure 4. 4. Thermal stability of bare Si and Ti_xSi_y-coated Si electrodes. (A) DSC profiles of bare Si and Ti_xSi_y-coated Si electrodes. (B) Schematic illustration showing the thermal decomposition reactions of an electrolyte with lithiated Si at elevated temperatures.

this point of view, it can be expected that the Ti_xSi_y coating layer on Si anode materials improve battery safety because the exothermic heat evolution (324 J /g) in the overall 80-320 ^oC was greatly reduced compared to non-coated Si electrodes (912 J /g).

4. Conclusion

In summary, we successfully synthesized titanium silicide coated silicon particles via a silicothermic reduction process of Si and TiO_2. The TiO_2 layers were conformally coated on the surface of Si in a solution, and subsequent thermal annealing led to a formation of titanium silicide coated Si particles. Since titanium silicide are electrically conductive and form a highly stable SEI layer, Ti_xSi_y-coated Si electrodes exhibit high electrochemical performances, including a high specific capacity and an excellent rate capability. Also, the Ti_xSi_y-coated Si electrodes showed significantly improved thermal stability, compared to non-coated Si electrodes. This process opens up a way to make other silicon-based anode materials for high performance lithium-ion batteries.

5. References

[1] J. M. Tarascon, M. Armand, *Nature* **2001**, *414*, 359-367.

[2] P. G. Bruce, B. Scrosati, J.-M. Tarascon, *Angew. Chem., Int. Ed.* **2008**, *47*, 2930-2946.

[3] M. S. Whittingham, *Chem. Rev.* **2004**, *104*, 4271-4302.

[4] C. K. Chan, H. Peng, G. Liu, K. McIlwrath, X. F. Zhang, R. A. Huggins, Y. Cui, *Nat. Nanotch.* **2008**, 3, 31-35.

[5] A. Magasinski, P. Dixon, B. Herzberg, A. Kvit, J. Ayala, G. Yushin, *Nat. Mater.* **2010**, *9*, 353-358.

[6] T. D. Hatchard, J. R. Dahn, *J. Electrochem. Soc.* **2004** , *151*, A838-A842.

[7] M. N. Obrovac, L. J. Krause, *J. Electrochem. Soc.* **2007**, *154*, A103-A108.

[8] X. H. Liu, L. Q. Zhang, , L. Zhong, Y. Liu, H. Zheng, J. W. Wang, J. H. Cho, S. A. Dayeh, S. T. Picraux, J. P. Sullivan, S. X. Mao, Z. Z. Ye, J. Y. Huang, *Nano Lett.* **2011** , *11* , 2251-2258

[9] U. Kasavajjula, C. Wang, A. J. Appleby, *J. Power Sources* **2007**, *163*, 1003-1039.

[10] H. Li, Z. X. Wang, L. Chen, X. J. Huang, *Adv. Mater.* **2009**, *21*, 4593-4607 .

[11] Y. S. Hu, R. Demir-Cakan, M.-M. Titirici, J. O. Muller, R. Schlogl, M. Antonietti, J. Maier, *Angew. Chem. Int. Ed.* **2008**, *47*, 1645-1649.

[12] P. F. Gao, J. W. Fu, J. Yang, R. G. Lu, J. L. Wang, X. Z. Tang, *Phys. Chem. Chem. Phys.* **2009**, *47*, 11101-.11105

[13] W. Wang, P. N. Kumta, *ACS Nano* **2009**, *4*, 2233-.2240

[14] B. M. Bang, H. Kim, J.-P. Lee, J. Cho, S. Park, *Energy Environ. Sci.* **2011**, *4*, 3395-3399.

[15] M.-H. Park, M. G. Kim, J. Joo, K. Kim, J. Kim, S. Ahn, Y. Cui, J. Cho, *Nano Lett.* **2009**, *9*, 3844-3847.

[16] H. Ma, F. Cheng, J. Chen, J. Zhao, C. Li, Z. Tao, J. Liang, *Adv. Mater.* **2007**, *19*, 4067-4070.

[17] H. Kim, B. Han, J. Choo, J. Cho, *Angew. Chem. Int. Ed.* **2008**, *47*, 10151-10154.

[18] Y. Yu, L. Gu, C. Zhu, S. Tsukimoto, P. A. van Aken, J. Maier, *Adv. Mater.* **2010**, *22*, 2247-2250.

[19] Y.-C. Yen, S.-C. Chao, H.-C. Wu, N.-L. Wu, *J. Electrochem. Soc.* **2009**, *156*, A95-A102

[20] Q. M. Pan, H. B. Wang, Y. H. Jiang, *Electrochem. Commun.* **2007**, *9*, 754-760.

[21] H. Yoo, J.-I. Lee, H. Kim, J.-P. Lee, J. Cho, S. Park, *Nano Lett.* **2011**, *11*, 4324-4328.

[22] L. F. Cui, Y. Yang, C. M. Hsu, Y. Cui, *Nano Lett.* **2009**, *9*, 3370-3374.

[23] Y. S. Hu, P. Adelhelm, B. M. Smarsly, J. Maier, *ChemSusChem* **2010**, *3*, 231-235.

[24] S. Murugesan, J. T. Harris, B. A. Korgel, K. J. Stevenson, *Chem. Mater.* **2012**, *24*, 1306-1315.

[25] Y. L. Kim, H. Y. Lee, S. W. Jang, S. H. Lim, S. J. Lee, H. K. Baik, Y. S. Yoon, S. M. Lee, *Electrochim. Acta* **2003**, *48*, 2593-2597.

[26] X. L. Yang, Z. Y. Wen, S. H. Huang, X. J. Zhu, X. F. Zhang, *Solid State Ionics* **2006**, *177*, 2807-2810.

[27] J. B. Kim, H. Y. Lee, K. S. Lee, S. H. Lim, S. M. Lee, *Electrochem. Commun.* **2003**, *5*, 544-548.

[28] J. W. Kim, J. H. Ryu, K. T. Lee, S. M. Oh, *J. Power Sources* **2005**, *147*, 227-233.

[29] D. C. Johnson, J. M. Mosby, S. C. Riha, A. L. Prieto, *J. Mater. Chem.* **2010**, *20*, 1993-1998.

[30] Y. He, X. Yu, Y. Wang, H. Li, X. Huang, *Adv. Mater.* **2011**, *23*, 4938-4941.

[31] H. Wu, G. Chan, J. W. Choi, I. Ryu, Y. Yao, M. T. McDowell, S. W. Lee, A. Jackson, Y. Yang, L. Hu, Y. Cui, *Nat. Nanotechnol.* **2012**, *7*, 310-315.

[32] Y. Yao, N. Liu, M. T. McDowell, M. Pasta, Y. Cui, *Energy Environ. Sci.* **2012**, *5*, 7927-7230.

[33] Z. P. GuO, J. Z. Wang, H. K. Liu, S. X. Dou, *J. Power Sources* **2005**, *146*, 448-451.

[34] R. W. Mann, L. A. Clevenger, P. D. Agnello, F. R. White, *IBM J. Res. Dev.* **1995**, *39*, 403-417.

[35] Z. Ma, L. H. Allen, D. D. J. Allman, *Appl. Phys. Lett.* **1995**, *77*, 4383-4390.

[36] S. Zhou, X. Liu, D. Wang, *Nano Lett.* **2010**, *10*, 860-863.

[37] T. B. Massalsky, *Binary Alloy Phase Diagram*, ASM, **1990**, 3370-3383.

[38] Z. Jiang, X. Dai, H. Middleton, *Mater. Sci. Eng. B* **2011**, *176*, 79-84.

[39] P. M. Kumar, S. Badrinarayanan, M. Sastry, *Thin Solid Films* **2000**, *358*, 122-130.

[40] G. B. Song, H. Joly, F. S. Liu, T. J. Peng, P. Wan, J. K. Liang, *Appl. Surf. Sci.* **2003**, *220*, 159-168.

[41] M. Berti, A. V. Drigo, C. Cohen, J. Siejka, G. G. Bentini, R. Nipoti, S. Guerri, *J. Appl. Phys.* **1984**, *55*, 3558-.3565

[42] F. Zhao, X. Cui, B. Wang, J. G. Hou, *Appl. Surf. Sci.* **2006**, *253*, 2785-2791.

[43] N.-S. I. A. Profatilova, S.-S. Kim, E.-H. Song, *Thermochim. Acta* **2008**, *480*, 10-